Star-Shaped Wheel for Mechanical Micro-Doppler Modulation

Journal:	*IEEE Antennas and Wireless Propagation Letters*
Manuscript ID	Draft
Manuscript Type:	Original Manuscript
Date Submitted by the Author:	n/a
Complete List of Authors:	Verdú Tirado, Jordi; Universitat Autonoma de Barcelona, Telecommunications and Systems Engineering Guerrero, Eloi; Universitat Autonoma de Barcelona, Telecommunications and Systems Engineering Parrón, Josep; Universitat Autònoma de Barcelona, Department of Telecommunication and System Engineering Lazaro, Antonio; Universitat Rovira i Virgili, DEEEA de Paco, Pedro; Autonomous University of Barcelona
Keywords:	Frequency-Modulated Coninuous Wave, Micro-Doppler, Radar
Note: The following files were submitted by the author for peer review, but cannot be converted to PDF. You must view these files (e.g. movies) online.	
Star_shaped_Doppler_Wheel_V2.tex	

Star-Shaped Wheel for Mechanical Micro-Doppler Modulation

Jordi Verdú, *Senior, IEEE,* Eloi Guerrero, *Student Member, IEEE,* Josep Parrón, Antonio Lázaro, *Senior, IEEE* and Pedro de Paco, *Senior, IEEE*

***Abstract*—This paper investigates the possibility of using deliberated geometries for rotating targets which may improve the detectability and classification by means of its micro-Doppler signature. Beyond the signature provided by the rotation rate of the target, every particular geometry leads to specific and unique modulation waveforms that increase the information related to this target. Different star-shaped wheels with particular geometries have been designed demonstrating different reflection characteristics and modulation waveforms. The signature of these rotating star-shaped wheels has been measured in an anechoic chamber using a general purpose 24 GHz FMCW radar platform and a detection algorithm based on the derivative of the cross-correlation is proposed which validates the proposed approach.**

***Index Terms*—Frequency-Modulated Continuous Wave, Micro-Doppler, Radar**

I. Introduction

COMPARED with other radar configurations, Frequency-Modulated Continous Wave (FMCW) radars allow micro-dynamics (vibrations, rotations) identification due to their capability in micro-Doppler detection beyond range and relative velocity. The working principle of a FMCW radar is based on the transmission of a continuous frequency-modulated microwave signal that will be later mixed with the signal reflected from the target. Phase variations in consecutive chirp ramps provide precise information about a specific target reaching sub-λ resolution [1]. FMCW radars have been successfully used in human target detection and classification applications related to autonomous vehicle [2], [3], medical monitoring [4], [5], or retrieval of audio signals by measuring micro-vibrations [6] among others.

Micro-Doppler phenomena is related to a frequency modulation in the reflected signal when the target is under certain mechanical vibration or rotation. This feature has been very useful in order to classify or recognize the nature of different objects since the micro-Doppler signature can be related to specific geometric or dynamic characteristics [7]–[10]. The rotation-induced micro-Doppler modulation occurs when a certain target moves from a given position to a new one describing a rotation around a reference axis as it is the case of rotating blades [11], [12].

J. Verdú, E. Guerrero, J. Parrón and P. de Paco are with the Department of Telecommunications and Systems Engineering, Universitat Autònoma de Barcelona. 08193 Cerdanyola del Vallès, Spain: (Jordi.Verdu@uab.cat).

A. Lázaro is with the Electronics, Electrical and Automatics Engineering Department, Universitat Rovira i Virgili. 43007 Tarragona, Spain.

This work has been supported by the Spanish Secretaría de Estado de Investigación, Desarrollo e Innovación under Grant RTI2018-096019-B-C33.

Manuscript received April 19, 2005; revised August 26, 2015.

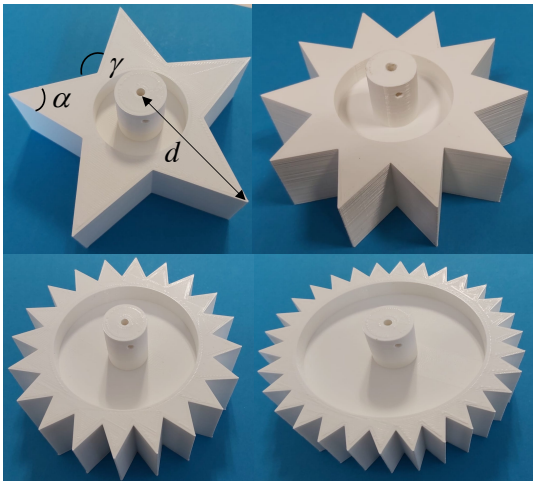

Fig. 1. 3D manufactured 5, 10, 20 and 30 tip star-shaped wheels.

Beyond the dynamic analysis of previous works, in this contribution we analyze, simulate and validate how the shape of the rotating target determines the time-dependent radar cross section (RCS) which takes the role of the modulation waveform. The spectrum of the IF signal is not only determined by the frequency allocation of side lobes, given by the rotation rate, but also by the amplitude which is directly related to the time-dependent RCS. This particular feature can be of interest in some applications, such as automotive radars, where unique micro-Doppler signatures can be generated to identify objects on the road and/or to avoid spoofing attacks.

In previous works [13], [14], it has been demonstrated that rotating elements can be used as warning signals. In this work, instead of using 90 degrees rotating dihedral reflection corners, the influence of star-shaped geometries is investigated to obtain additional information from the target and thus improve the detectability. Taking advantage on the additive 3D manufacturing technologies, different star-shaped wheels in Fig. 1 have been designed with the objective to provide particular and specific modulation micro-Doppler signals by means of the particular time-dependent RCS. The wheels have been covered by an adhesive cooper layer to increase the reflectivity of the targets.

Since the modulation signal is mechanically generated, it is independent from operating frequency which may hinder electronic designs at high frequencies, for example in the 77 GHz band. Since the objective is to use these targets as a warning signals, the received IF signal will be known a priori, therefore, similarly to [15], a method based on the derivative

of the cross-correlation between the reference (simulated) and the received (measured) has been implemented.

This contribution is organized as follows, the theoretical analysis of the received IF signal is carried out considering the time-dependence of the RCS is found in Section II. In Section III it is compared the previous simulation results with the measurements of rotating star-shaped wheels on an anechoic chamber with a 24 GHz FMCW radar. In Section IV an algorithm is proposed to carry out the signal detection based on the cross-correlation. Finally, the conclusions are presented in section V.

II. Mechanical Modulation by means of Time-dependent RCS

The basic mode of operation of the FMCW radar consists in the transmission of L chirps of duration T_c which will be later translated to intermediate frequency (IF). The chirp signal is defined by an amplitude A, the carrier frequency f_c and the chirp sweeping slope $\mu = B/T_c$, being B the bandwidth. The received signal will be delayed with an amplitude proportional to the radar cross-section σ of the target. For a simplified rotating target modelled using N backscatters, the IF signal can be obtained by the contribution of each one as [13],

$$x_{IF}(t) = A\sqrt{\sigma(t)}\prod\left(\frac{t}{T_c}\right)e^{-j2\pi\left(f_c\tau-\frac{\mu\tau^2}{2}\right)}e^{-j2\pi\mu\tau t} \quad (1)$$

In the case of the 90 degrees rotating dihedral reflection corners, the modulation waveform is very similar to an on-off keying (OOK) ASK modulation which is modelled by the term $e^{-j\beta\sin(\Omega_r t+\theta_0)}$ as developed in [13], where $\beta = 4\pi d/\lambda$ is the modulation index in FM signals (being d the radius of the wheel), and Ω_r is the rotation rate. However, our star-shaped wheel cannot be modelled in the same way because the walls reflect the incident electric field in a particular direction, or generate internal reflections between adjacent walls, triggering destructive or constructive interferences in the LOS of the radar. Therefore, the geometry of the target will have an influence on the modulation waveform. Due to the time-dependence of the RCS the theoretical approach in (1) is not precise enough to properly model the received IF signal.

To analyze the impact of the RCS on the received IF signal, four different star-shaped wheels with 5, 10, 20 and 30 tips, shown in Fig. 1, have been designed with radius d = 5.6 cm and tip angle α = 24° in all of them. With this geometric definition, the angle between adjacent walls γ is different in all the wheels and so is the corresponding RCS. The monostatic RCS has been obtained for each wheel by means of 3D simulation using FEKO software [16] as shown in Fig. 2. The incident angle at which maximum reflection occurs is different in all of them, as well as the monostatic RCS periodicity which is related to the number of tips N. Fig. 2 shows that all wheels generate strong echoes for that incident angles where one wall is perpendicular to the LOS of the radar.

Taking into account the size of the target, d = 5.6 cm, as well as the operating frequency 24 GHz, far-field conditions can be assumed so the monostatic RCS in Fig. 3 is used to model the received IF signal. Otherwise, in a near-field scenario, the

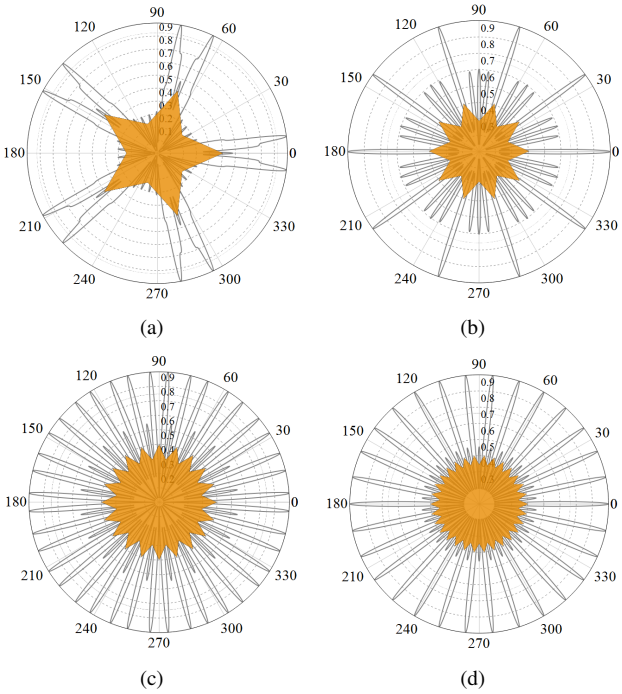

Fig. 2. Normalised polar representation of the monostatic RCS for the (a) 5 tip, (b) 10 tip, (c) 20 tip and (d) 30 tip star-shaped wheels respectively.

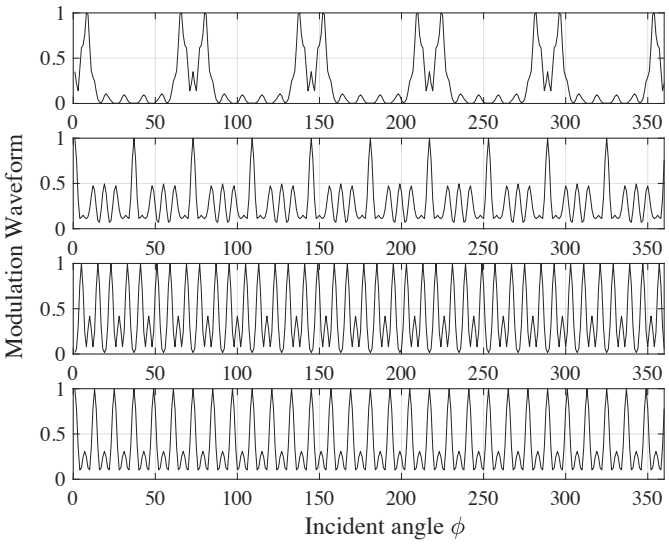

Fig. 3. Obtained RCS for the different wheels as a function of the incident angle ϕ. From top to bottom 5, 10, 20 and 30 tip star-shaped wheels.

RCS should be computed as the integration of the electric field in the radiation pattern of the antenna. The resulting RCS has been normalized with respect its maximum value with the aim to compare the behaviour among the different wheels. The RCS is periodic for all the wheels. Depending on the angle between adjacent walls the number of RCS peaks can be N (N = 10 and 30) or $2N$ (N = 5 and 20). Of course, different geometries would lead different RCS behavior. This is an interesting feature to improve recognition.

Without loss of generality, the 20 tips star-shaped wheel has

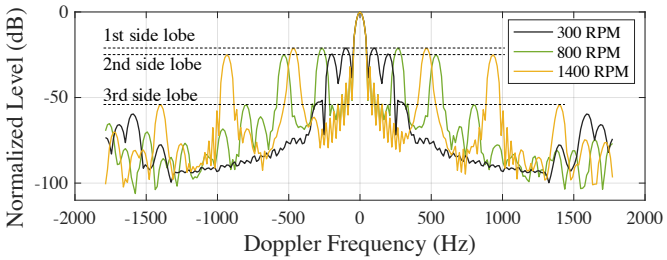

Fig. 4. Simulated received signal for 300 (solid black), 800 (dashed green) and 1400 (solid yellow) RPMs in the 20 tip star-shaped wheel.

been simulated using different rotation rates Ω_r = 300, 800 and 1400 RPM. As shown in Fig. 4, and using the obtained RCS in Fig. 3 as modulation waveform, first side lobes are found at 100Hz, 266 Hz and 466 Hz respectively, being the consecutive second and third side lobes separated by $N\Omega_r$ which is in agreement with results in [17]. It is also important to highlight that the amplitude of side lobes does not depend on the Ω_r. The amplitude for first, second and third side lobes is coincident for all the rotation rates, and only depends on the modulation waveform. For $\Omega_r = 300$ RPM, the amplitude of the third side lobe is not perfectly aligned with the others as it occurs for higher rotation rates. This is due to the fact that this side lobe is approximately allocated in the limit of the modulation bandwidth which can be approximated as Bw $\approx 2(\beta+1)\Omega_r/2\pi$ [13]. For $\Omega_r = 300$ RPM (5 Hz), the third ($k = 3$) side lobe is allocated at $k\Omega_r N = 300$ Hz, being Bw $\approx$ 580 Hz (with $d = 5.7$ cm and f_0 = 24 GHz).

From simulation results, it can be concluded that there is a trade-off between the rotation rate Ω_r, the radius d of the star-shaped wheel, and thus the modulation index β, for the detection or recognition of side lobes. For low Ω_r, it will be interesting to use star-shaped wheels with large number of tips N to increase separation between side lobes and facilitate the detection, and small N when the rotation rate is high. In case of using large N at high rotation rates, it will be necessary to use large values of d to increase the modulation bandwidth for detecting side lobes.

III. Measurements and Characterization of Star-shaped Wheels

For the experimental set-up, each wheel with $N = 5$, 10, 20 and 30 tips, has been mounted on a generic current-controlled DC motor in order to characterize different rotating rates in an anechoic chamber. The measurement set-up is shown in Fig. 5, where the distance between the radar and the rotating wheel is $R_0 = 2.6$ m. The measurements have been carried out using a general purpose 24 GHz FMCW DemoRad by Analog Devices and Inras. The operation bandwidth is 300 MHz leading to a velocity resolution of Δv = 0.162 m/s, equivalently Δf_D = 12.9 Hz for a $T_c = 280$ μs.

The 5, 10, 20 and 30 tip star-shaped wheels have been measured at Ω_r = 1000, 1100, 1400 and 1550 RPMs respectively. As shown in Fig. 6, there is a good agreement with theoretical simulations. The allocation of the frequency lobes, given by the product $N\Omega_r$, agrees with the theoretical prediction. The

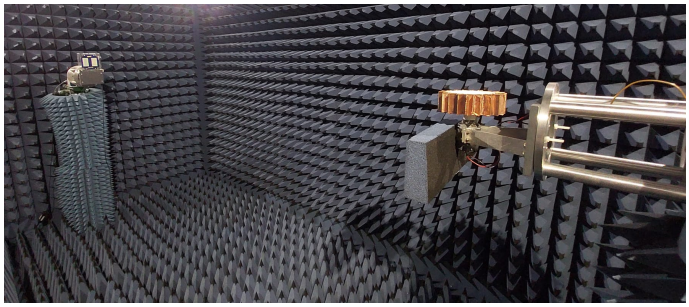

Fig. 5. Characterization set-up inside the anechoic chamber. The distance between the radar and the rotating wheel is $R_0 = 2.6$ m.

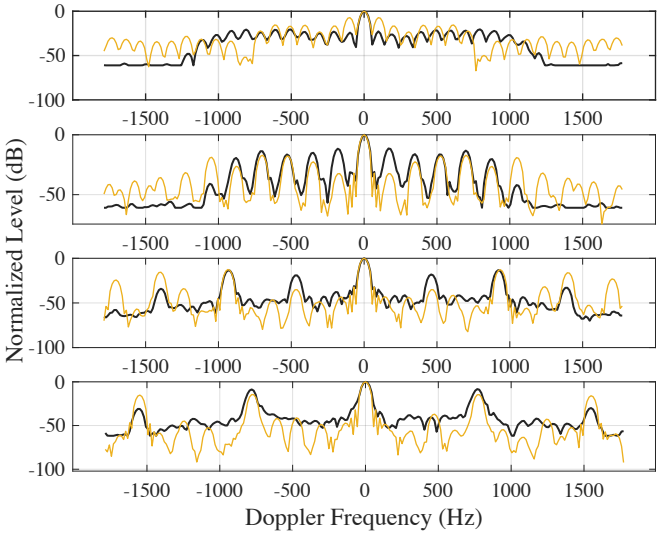

Fig. 6. Comparison between measurement (black) and simulation (yellow) received signal for the 5 (@1000RPM), 10 (@1100RPM), 20 (@1400RPM) and 30 (@1550RPM) tip star-shaped wheels (from top to bottom).

discrepancy in the amplitude of some lobes may come from vibrations in the elevation plane due to some vibration in the plane of rotation non considered in the theoretical model. For sake of clarity in the comparison, the received signal level has been normalized in all cases.

IV. Method for Detection of Rotating Star-shaped Wheels

The use of particular shapes may be used to increase detectability. As it was previously commented, if a warning signal is expected, the reference signal will be known a priori. The good agreement between simulation and measurement, particularly, in the allocation of the frequency lobes as well as the modulation bandwidth allows to propose a detection method based on the derivative by finite differences of the cross-correlation $R_{zx}[n]$ in the discrete frequency domain between the reference (simulation) $X[n]$ and the received (measurement) signal $Z[n]$ as,

$$R_{xz}[n] = X[n] \star Z[n] \triangleq \sum_{m=-\infty}^{\infty} X^*[m]Z[m+n] \quad (2)$$

being * the conjugate operator.

Different experiments have been carried out in order to validate the proposed detection method. First, a reference signal corresponding to a 20-tip star-shaped wheel has been compared with the measurements for wheels with $N = 10$ (green), N =20 (yellow) and N =30 (purple) tips in Fig. 7(a). Since the wheels are different (different N), for the same Ω_r the lobes are not coincident. Therefore, different Ω_r has been set in each wheel (1250, 1380 and 1810 RPM respectively) in such a way some lobes are coincident with the lobes in the reference signal which increases the complexity in the detection of the target. The result of the cross-correlation R_{xz} shows that the highest value along the samples corresponds to the one related with the $N = 20$ tips wheel as expected. Moreover, the most interesting issue is the presence of peaks separated a distance of $N\Omega_r$, that is, at those positions where all the lobes are coincident. This only happens for the case where the number of tips as well as the rotation rate is coincident. Therefore, the derivative of the cross-correlation R'_{xz} can be used to determine the most-likely signal by the inspection of the peaks with the highest level as shown in the bottom of Fig. 7(a).

A second experiment has been carried out using the wheel with 20 tips with different rotation rates. The signal to be detected is the one provided by a wheel at 1380 RPM (yellow trace). A reference signal with 1400 RPM has been used (grey dot-dash line) which is slightly different from the signal to be detected to emulate some drift in the Ω_r value.

The cross-correlation R_{xz} shows the presence of different peaks as before. However, the measurements of wheels at 1100 and 800 RPM (green and blue respectively) result in a higher level of cross-correlation which may be not suitable to carry out a successful detection. However, as previously commented, the derivative provides unambiguous detection because the peaks only appear when the distance between lobes $N\Omega_r$ is coincident. This is shown in the bottom of Fig. 7(b) where the peaks with the highest level corresponds to the yellow trace, the one with the RPMs closer to the reference. Then, the peak detection can be easily associated to the expected signal to be received.

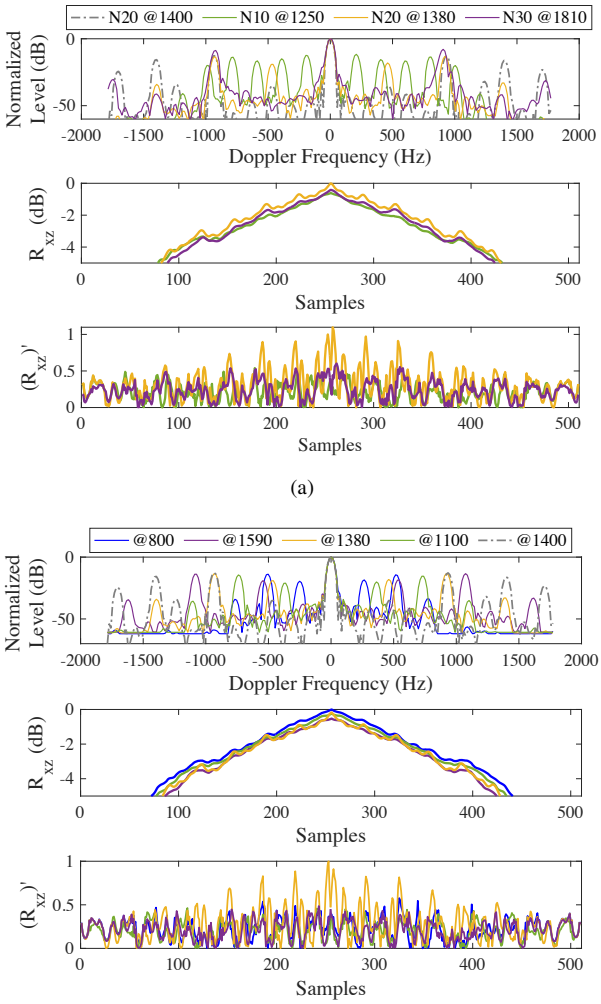

Fig. 7. (Top) Comparison between the reference signal (grey dot-dash line) and measured received signals, (middle) Cross-correlation between the reference signal and measurements, (bottom) derivative of the cross-correlation. (a) Results for star-shaped wheels with different number of tips N, (b) Results for a 20 tip wheel at different rotation rates.

V. Conclusion

In this paper, it has been demonstrated that specific geometric shapes may lead to a particular modulation waveform in rotating targets. To this aim, star-shaped wheels with different number of tips have been designed and tested. The allocation of the frequency side lobes in the IF signal is directly related to the rotation rate, being the separation determined by the product between the number of tips and the rotation rate. However, depending on the modulation waveform, given by a certain geometry, the amplitude of side lobes may be different and not dependent on the rotation rate. This particular behaviour may improve classification and identification of rotating targets. Simulation results have been validated by means of experimental characterization of different star-shaped wheels using a general purpose 24 GHz radar platform. A detection method based on the derivative of the cross-correlation of a reference signal and the signal to be detected has been proposed and succesfully validated. The method is suitable in case of star-shaped wheels with different number of tips although there is coincidence in some lobes, and also for the same wheel at different rotating rates which shows the reliability and robustness of the proposed approach.

Acknowledgment

The authors would like to thank the OpenLabs at Universitat Autònoma de Barcelona for the support in the manufacturing of the star-shaped wheels allowing the use of the additive manufacturing tools and techniques.

References

[1] M. Skolnik, *Introduction to radar systems*. Boston: McGraw Hill, 2001.
[2] E. Hyun, Y.-S. Jin, and J.-H. Lee, "Moving and stationary target detection scheme using coherent integration and subtraction for automotive FMCW radar systems," in *2017 IEEE Radar Conference (RadarConf)*. IEEE, may 2017.

[3] C. Will, P. Vaishnav, A. Chakraborty, and A. Santra, "Human target detection, tracking, and classification using 24-GHz FMCW radar," *IEEE Sensors Journal*, vol. 19, no. 17, pp. 7283–7299, sep 2019.
[4] M. Alizadeh, G. Shaker, J. C. M. D. Almeida, P. P. Morita, and S. Safavi-Naeini, "Remote monitoring of human vital signs using mm-wave FMCW radar," *IEEE Access*, vol. 7, pp. 54 958–54 968, 2019.
[5] H. Lee, B.-H. Kim, J.-K. Park, S. W. Kim, and J.-G. Yook, "A resolution enhancement technique for remote monitoring of the vital signs of multiple subjects using a 24 ghz bandwidth-limited FMCW radar," *IEEE Access*, vol. 8, pp. 1240–1248, 2020.
[6] E. Guerrero, J. Brugues, J. Verdu, and P. de Paco, "Microwave microphone using a general purpose 24-GHz FMCW radar," *IEEE Sensors Letters*, vol. 4, no. 6, pp. 1–4, jun 2020.
[7] V. Chen, F. Li, S.-S. Ho, and H. Wechsler, "Micro-doppler effect in radar: phenomenon, model, and simulation study," *IEEE Transactions on Aerospace and Electronic Systems*, vol. 42, no. 1, pp. 2–21, jan 2006.
[8] S. Ram and H. Ling, "Microdoppler signature simulation of computer animated human and animal motions," in *2008 IEEE Antennas and Propagation Society International Symposium*. IEEE, jul 2008.
[9] R. Mamgain, R. Jain, and D. Deb, "Study and simulation of radar targets micro-doppler signature," in *2018 International Conference on Radar (RADAR)*. IEEE, aug 2018.
[10] J. Gong, J. Yan, D. Li, R. Chen, F. Tian, and Z. Yan, "Theoretical and experimental analysis of radar micro-doppler signature modulated by rotating blades of drones," *IEEE Antennas and Wireless Propagation Letters*, vol. 19, no. 10, pp. 1659–1663, oct 2020.
[11] Z. Zhou and J. Huang, "X-band radar cross-section of tandem helicopter based on dynamic analysis approach," *Sensors*, vol. 21, no. 1, p. 271, jan 2021.
[12] T. Peto, S. Bilicz, L. Szucs, S. Gyimothy, and J. Pavo, "The radar cross section of small propellers on unmanned aerial vehicles," in *2016 10th European Conference on Antennas and Propagation (EuCAP)*. IEEE, apr 2016.
[13] A. Lazaro, M. Lazaro, R. Villarino, and P. D. Paco, "New radar micro-doppler tag for road safety based on the signature of rotating backscatters," *IEEE Sensors Journal*, vol. 21, no. 6, pp. 8604–8612, mar 2021.
[14] A. Lazaro, M. Lazaro, R. Villarino, D. Girbau, and P. de Paco, "Car2car communication using a modulated backscatter and automotive FMCW radar," *Sensors*, vol. 21, no. 11, p. 3656, may 2021.
[15] W. Y. Yang, J. H. Park, J. W. Bae, N. H. Myung, and C. H. Kim, "Automatic algorithm for estimating the jet engine blade number from the radar target signature of aircraft targets," *IEEE Aerospace and Electronic Systems Magazine*, vol. 30, no. 7, pp. 18–29, jul 2015.
[16] *www.altair.com/feko*.
[17] V. Chen, "Analysis of radar micro-doppler with time-frequency transform," in *Proceedings of the Tenth IEEE Workshop on Statistical Signal and Array Processing (Cat. No.00TH8496)*. IEEE, 2020.

Star-Shaped Wheel for Mechanical Micro-Doppler Modulation

Jordi Verdú, *Senior, IEEE,* Eloi Guerrero, *Student Member, IEEE,* Josep Parrón, Antonio Lázaro, *Senior, IEEE* and Pedro de Paco, *Senior, IEEE*

***Abstract*—This paper investigates the possibility of using deliberated geometries for rotating targets which may improve the detectability and classification by means of its micro-Doppler signature. Beyond the signature provided by the rotation rate of the target, every particular geometry leads to specific and unique modulation waveforms that increase the information related to this target. Different star-shaped wheels with particular geometries have been designed demonstrating different reflection characteristics and modulation waveforms. The signature of these rotating star-shaped wheels has been measured in an anechoic chamber using a general purpose 24 GHz FMCW radar platform and a detection algorithm based on the derivative of the cross-correlation is proposed which validates the proposed approach.**

***Index Terms*—Frequency-Modulated Continuous Wave, Micro-Doppler, Radar**

I. Introduction

COMPARED with other radar configurations, Frequency-Modulated Continous Wave (FMCW) radars allow micro-dynamics (vibrations, rotations) identification due to their capability in micro-Doppler detection beyond range and relative velocity. The working principle of a FMCW radar is based on the transmission of a continuous frequency-modulated microwave signal that will be later mixed with the signal reflected from the target. Phase variations in consecutive chirp ramps provide precise information about a specific target reaching sub-λ resolution [1]. FMCW radars have been successfully used in human target detection and classification applications related to autonomous vehicle [2], [3], medical monitoring [4], [5], or retrieval of audio signals by measuring micro-vibrations [6] among others.

Micro-Doppler phenomena is related to a frequency modulation in the reflected signal when the target is under certain mechanical vibration or rotation. This feature has been very useful in order to classify or recognize the nature of different objects since the micro-Doppler signature can be related to specific geometric or dynamic characteristics [7]–[10]. The rotation-induced micro-Doppler modulation occurs when a certain target moves from a given position to a new one describing a rotation around a reference axis as it is the case of rotating blades [11], [12].

J. Verdú, E. Guerrero, J. Parrón and P. de Paco are with the Department of Telecommunications and Systems Engineering, Universitat Autònoma de Barcelona. 08193 Cerdanyola del Vallès, Spain: (Jordi.Verdu@uab.cat).

A. Lázaro is with the Electronics, Electrical and Automatics Engineering Department, Universitat Rovira i Virgili. 43007 Tarragona, Spain.

This work has been supported by the Spanish Secretaría de Estado de Investigación, Desarrollo e Innovación under Grant RTI2018-096019-B-C33.

Manuscript received April 19, 2005; revised August 26, 2015.

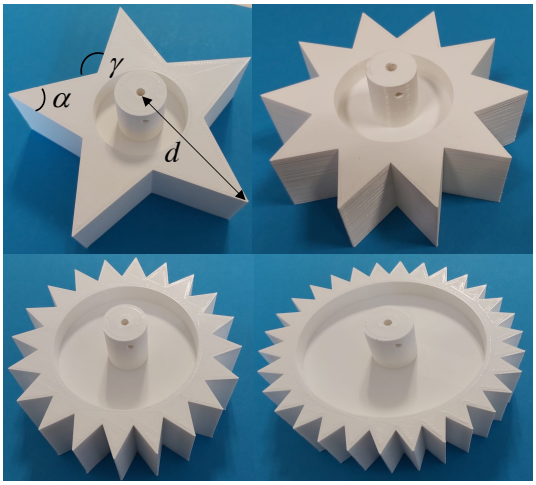

Fig. 1. 3D manufactured 5, 10, 20 and 30 tip star-shaped wheels.

Beyond the dynamic analysis of previous works, in this contribution we analyze, simulate and validate how the shape of the rotating target determines the time-dependent radar cross section (RCS) which takes the role of the modulation waveform. The spectrum of the IF signal is not only determined by the frequency allocation of side lobes, given by the rotation rate, but also by the amplitude which is directly related to the time-dependent RCS. This particular feature can be of interest in some applications, such as automotive radars, where unique micro-Doppler signatures can be generated to identify objects on the road and/or to avoid spoofing attacks.

In previous works [13], [14], it has been demonstrated that rotating elements can be used as warning signals. In this work, instead of using 90 degrees rotating dihedral reflection corners, the influence of star-shaped geometries is investigated to obtain additional information from the target and thus improve the detectability. Taking advantage on the additive 3D manufacturing technologies, different star-shaped wheels in Fig. 1 have been designed with the objective to provide particular and specific modulation micro-Doppler signals by means of the particular time-dependent RCS. The wheels have been covered by an adhesive cooper layer to increase the reflectivity of the targets.

Since the modulation signal is mechanically generated, it is independent from operating frequency which may hinder electronic designs at high frequencies, for example in the 77 GHz band. Since the objective is to use these targets as a warning signals, the received IF signal will be known a priori, therefore, similarly to [15], a method based on the derivative

of the cross-correlation between the reference (simulated) and the received (measured) has been implemented.

This contribution is organized as follows, the theoretical analysis of the received IF signal is carried out considering the time-dependence of the RCS is found in Section II. In Section III it is compared the previous simulation results with the measurements of rotating star-shaped wheels on an anechoic chamber with a 24 GHz FMCW radar. In Section IV an algorithm is proposed to carry out the signal detection based on the cross-correlation. Finally, the conclusions are presented in section V.

II. Mechanical Modulation by means of Time-dependent RCS

The basic mode of operation of the FMCW radar consists in the transmission of L chirps of duration T_c which will be later translated to intermediate frequency (IF). The chirp signal is defined by an amplitude A, the carrier frequency f_c and the chirp sweeping slope $\mu = B/T_c$, being B the bandwidth. The received signal will be delayed with an amplitude proportional to the radar cross-section σ of the target. For a simplified rotating target modelled using N backscatters, the IF signal can be obtained by the contribution of each one as [13],

$$x_{IF}(t) = A\sqrt{\sigma(t)}\prod\left(\frac{t}{T_c}\right)e^{-j2\pi\left(f_c\tau-\frac{\mu\tau^2}{2}\right)}e^{-j2\pi\mu\tau t} \quad (1)$$

In the case of the 90 degrees rotating dihedral reflection corners, the modulation waveform is very similar to an on-off keying (OOK) ASK modulation which is modelled by the term $e^{-j\beta\sin(\Omega_r t+\theta_0)}$ as developed in [13], where $\beta = 4\pi d/\lambda$ is the modulation index in FM signals (being d the radius of the wheel), and Ω_r is the rotation rate. However, our star-shaped wheel cannot be modelled in the same way because the walls reflect the incident electric field in a particular direction, or generate internal reflections between adjacent walls, triggering destructive or constructive interferences in the LOS of the radar. Therefore, the geometry of the target will have an influence on the modulation waveform. Due to the time-dependence of the RCS the theoretical approach in (1) is not precise enough to properly model the received IF signal.

To analyze the impact of the RCS on the received IF signal, four different star-shaped wheels with 5, 10, 20 and 30 tips, shown in Fig. 1, have been designed with radius d = 5.6 cm and tip angle α = 24° in all of them. With this geometric definition, the angle between adjacent walls γ is different in all the wheels and so is the corresponding RCS. The monostatic RCS has been obtained for each wheel by means of 3D simulation using FEKO software [16] as shown in Fig. 2. The incident angle at which maximum reflection occurs is different in all of them, as well as the monostatic RCS periodicity which is related to the number of tips N. Fig. 2 shows that all wheels generate strong echoes for that incident angles where one wall is perpendicular to the LOS of the radar.

Taking into account the size of the target, d = 5.6 cm, as well as the operating frequency 24 GHz, far-field conditions can be assumed so the monostatic RCS in Fig. 3 is used to model the received IF signal. Otherwise, in a near-field scenario, the

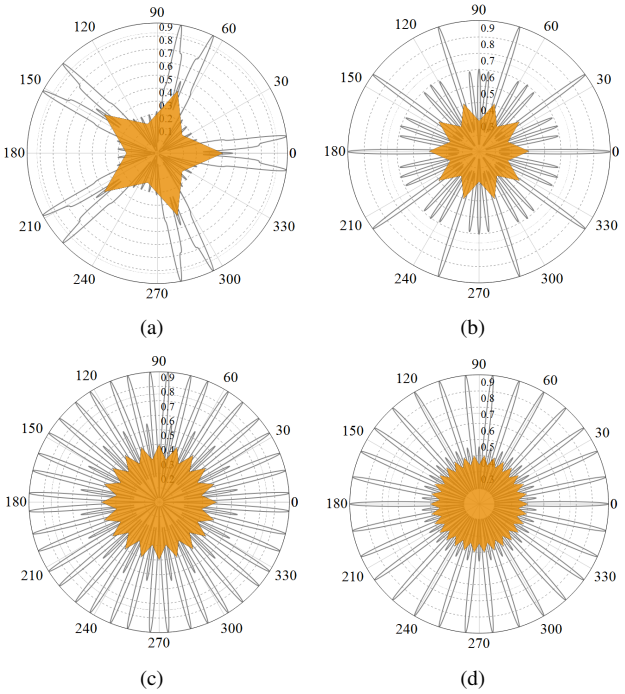

Fig. 2. Normalised polar representation of the monostatic RCS for the (a) 5 tip, (b) 10 tip, (c) 20 tip and (d) 30 tip star-shaped wheels respectively.

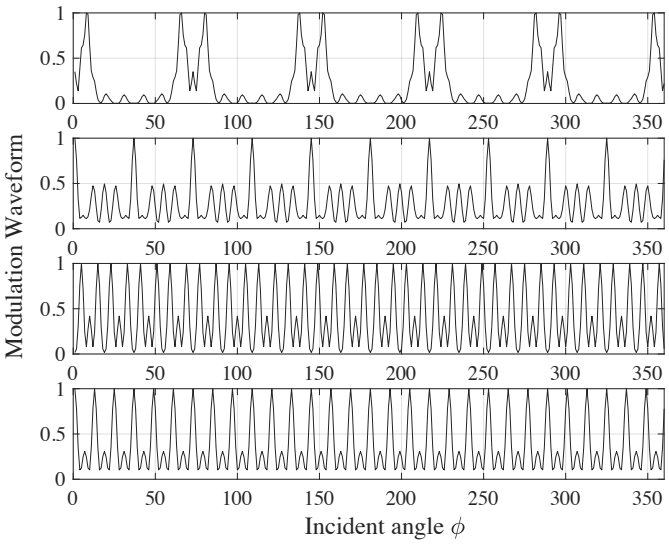

Fig. 3. Obtained RCS for the different wheels as a function of the incident angle ϕ. From top to bottom 5, 10, 20 and 30 tip star-shaped wheels.

RCS should be computed as the integration of the electric field in the radiation pattern of the antenna. The resulting RCS has been normalized with respect its maximum value with the aim to compare the behaviour among the different wheels. The RCS is periodic for all the wheels. Depending on the angle between adjacent walls the number of RCS peaks can be N (N = 10 and 30) or $2N$ (N = 5 and 20). Of course, different geometries would lead different RCS behavior. This is an interesting feature to improve recognition.

Without loss of generality, the 20 tips star-shaped wheel has

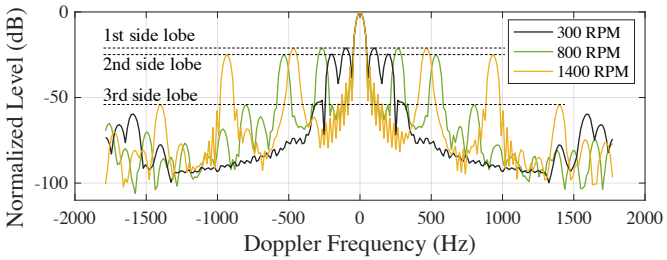

Fig. 4. Simulated received signal for 300 (solid black), 800 (dashed green) and 1400 (solid yellow) RPMs in the 20 tip star-shaped wheel.

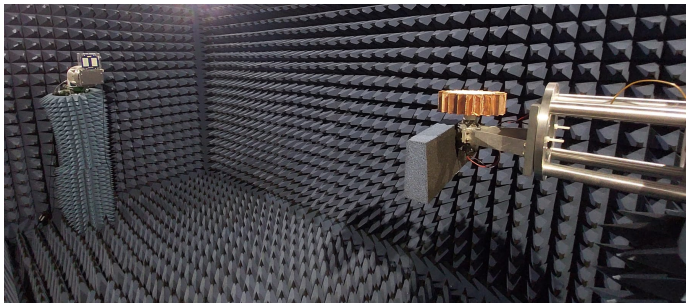

Fig. 5. Characterization set-up inside the anechoic chamber. The distance between the radar and the rotating wheel is $R_0 = 2.6$ m.

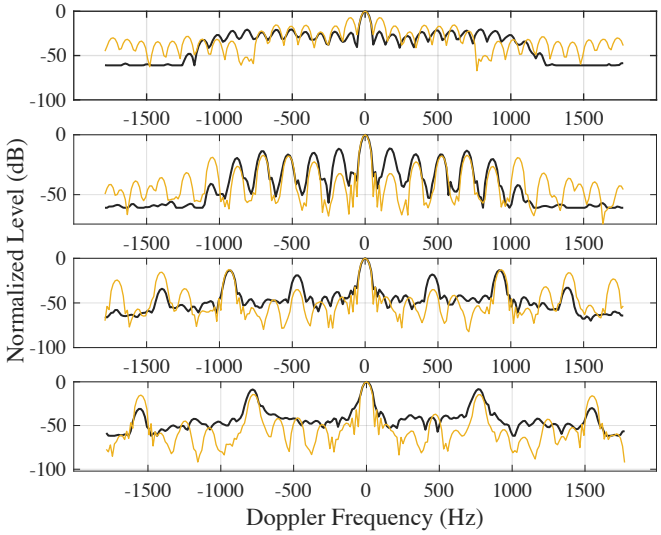

Fig. 6. Comparison between measurement (black) and simulation (yellow) received signal for the 5 (@1000RPM), 10 (@1100RPM), 20 (@1400RPM) and 30 (@1550RPM) tip star-shaped wheels (from top to bottom).

been simulated using different rotation rates Ω_r = 300, 800 and 1400 RPM. As shown in Fig. 4, and using the obtained RCS in Fig. 3 as modulation waveform, first side lobes are found at 100Hz, 266 Hz and 466 Hz respectively, being the consecutive second and third side lobes separated by $N\Omega_r$ which is in agreement with results in [17]. It is also important to highlight that the amplitude of side lobes does not depend on the Ω_r. The amplitude for first, second and third side lobes is coincident for all the rotation rates, and only depends on the modulation waveform. For $\Omega_r = 300$ RPM, the amplitude of the third side lobe is not perfectly aligned with the others as it occurs for higher rotation rates. This is due to the fact that this side lobe is approximately allocated in the limit of the modulation bandwidth which can be approximated as Bw $\approx 2(\beta+1)\Omega_r/2\pi$ [13]. For $\Omega_r = 300$ RPM (5 Hz), the third ($k = 3$) side lobe is allocated at $k\Omega_r N = 300$ Hz, being Bw ≈ 580 Hz (with $d = 5.7$ cm and f_0 = 24 GHz).

From simulation results, it can be concluded that there is a trade-off between the rotation rate Ω_r, the radius d of the star-shaped wheel, and thus the modulation index β, for the detection or recognition of side lobes. For low Ω_r, it will be interesting to use star-shaped wheels with large number of tips N to increase separation between side lobes and facilitate the detection, and small N when the rotation rate is high. In case of using large N at high rotation rates, it will be necessary to use large values of d to increase the modulation bandwidth for detecting side lobes.

III. Measurements and Characterization of Star-shaped Wheels

For the experimental set-up, each wheel with $N = 5$, 10, 20 and 30 tips, has been mounted on a generic current-controlled DC motor in order to characterize different rotating rates in an anechoic chamber. The measurement set-up is shown in Fig. 5, where the distance between the radar and the rotating wheel is $R_0 = 2.6$ m. The measurements have been carried out using a general purpose 24 GHz FMCW DemoRad by Analog Devices and Inras. The operation bandwidth is 300 MHz leading to a velocity resolution of Δv = 0.162 m/s, equivalently Δf_D = 12.9 Hz for a $T_c = 280$ μs.

The 5, 10, 20 and 30 tip star-shaped wheels have been measured at Ω_r = 1000, 1100, 1400 and 1550 RPMs respectively. As shown in Fig. 6, there is a good agreement with theoretical simulations. The allocation of the frequency lobes, given by the product $N\Omega_r$, agrees with the theoretical prediction. The discrepancy in the amplitude of some lobes may come from vibrations in the elevation plane due to some vibration in the plane of rotation non considered in the theoretical model. For sake of clarity in the comparison, the received signal level has been normalized in all cases.

IV. Method for Detection of Rotating Star-shaped Wheels

The use of particular shapes may be used to increase detectability. As it was previously commented, if a warning signal is expected, the reference signal will be known a priori. The good agreement between simulation and measurement, particularly, in the allocation of the frequency lobes as well as the modulation bandwidth allows to propose a detection method based on the derivative by finite differences of the cross-correlation $R_{zx}[n]$ in the discrete frequency domain between the reference (simulation) $X[n]$ and the received (measurement) signal $Z[n]$ as,

$$R_{xz}[n] = X[n] \star Z[n] \triangleq \sum_{m=-\infty}^{\infty} X^*[m]Z[m+n] \quad (2)$$

being * the conjugate operator.

Different experiments have been carried out in order to validate the proposed detection method. First, a reference signal corresponding to a 20-tip star-shaped wheel has been compared with the measurements for wheels with $N = 10$ (green), $N = 20$ (yellow) and $N = 30$ (purple) tips in Fig. 7(a). Since the wheels are different (different N), for the same Ω_r the lobes are not coincident. Therefore, different Ω_r has been set in each wheel (1250, 1380 and 1810 RPM respectively) in such a way some lobes are coincident with the lobes in the reference signal which increases the complexity in the detection of the target. The result of the cross-correlation R_{xz} shows that the highest value along the samples corresponds to the one related with the $N = 20$ tips wheel as expected. Moreover, the most interesting issue is the presence of peaks separated a distance of $N\Omega_r$, that is, at those positions where all the lobes are coincident. This only happens for the case where the number of tips as well as the rotation rate is coincident. Therefore, the derivative of the cross-correlation R'_{xz} can be used to determine the most-likely signal by the inspection of the peaks with the highest level as shown in the bottom of Fig. 7(a).

A second experiment has been carried out using the wheel with 20 tips with different rotation rates. The signal to be detected is the one provided by a wheel at 1380 RPM (yellow trace). A reference signal with 1400 RPM has been used (grey dot-dash line) which is slightly different from the signal to be detected to emulate some drift in the Ω_r value.

The cross-correlation R_{xz} shows the presence of different peaks as before. However, the measurements of wheels at 1100 and 800 RPM (green and blue respectively) result in a higher level of cross-correlation which may be not suitable to carry out a successful detection. However, as previously commented, the derivative provides unambiguous detection because the peaks only appear when the distance between lobes $N\Omega_r$ is coincident. This is shown in the bottom of Fig. 7(b) where the peaks with the highest level corresponds to the yellow trace, the one with the RPMs closer to the reference. Then, the peak detection can be easily associated to the expected signal to be received.

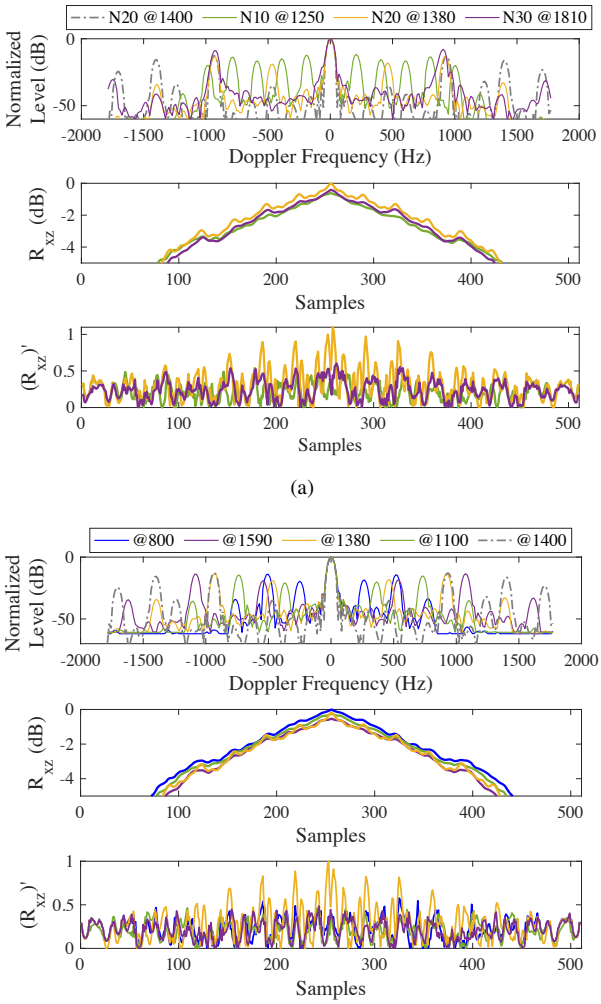

Fig. 7. (Top) Comparison between the reference signal (grey dot-dash line) and measured received signals, (middle) Cross-correlation between the reference signal and measurements, (bottom) derivative of the cross-correlation. (a) Results for star-shaped wheels with different number of tips N, (b) Results for a 20 tip wheel at different rotation rates.

V. Conclusion

In this paper, it has been demonstrated that specific geometric shapes may lead to a particular modulation waveform in rotating targets. To this aim, star-shaped wheels with different number of tips have been designed and tested. The allocation of the frequency side lobes in the IF signal is directly related to the rotation rate, being the separation determined by the product between the number of tips and the rotation rate. However, depending on the modulation waveform, given by a certain geometry, the amplitude of side lobes may be different and not dependent on the rotation rate. This particular behaviour may improve classification and identification of rotating targets. Simulation results have been validated by means of experimental characterization of different star-shaped wheels using a general purpose 24 GHz radar platform. A detection method based on the derivative of the cross-correlation of a reference signal and the signal to be detected has been proposed and succesfully validated. The method is suitable in case of star-shaped wheels with different number of tips although there is coincidence in some lobes, and also for the same wheel at different rotating rates which shows the reliability and robustness of the proposed approach.

Acknowledgment

The authors would like to thank the OpenLabs at Universitat Autònoma de Barcelona for the support in the manufacturing of the star-shaped wheels allowing the use of the additive manufacturing tools and techniques.

References

[1] M. Skolnik, *Introduction to radar systems*. Boston: McGraw Hill, 2001.
[2] E. Hyun, Y.-S. Jin, and J.-H. Lee, "Moving and stationary target detection scheme using coherent integration and subtraction for automotive FMCW radar systems," in *2017 IEEE Radar Conference (RadarConf)*. IEEE, may 2017.

[3] C. Will, P. Vaishnav, A. Chakraborty, and A. Santra, "Human target detection, tracking, and classification using 24-GHz FMCW radar," *IEEE Sensors Journal*, vol. 19, no. 17, pp. 7283–7299, sep 2019.
[4] M. Alizadeh, G. Shaker, J. C. M. D. Almeida, P. P. Morita, and S. Safavi-Naeini, "Remote monitoring of human vital signs using mm-wave FMCW radar," *IEEE Access*, vol. 7, pp. 54 958–54 968, 2019.
[5] H. Lee, B.-H. Kim, J.-K. Park, S. W. Kim, and J.-G. Yook, "A resolution enhancement technique for remote monitoring of the vital signs of multiple subjects using a 24 ghz bandwidth-limited FMCW radar," *IEEE Access*, vol. 8, pp. 1240–1248, 2020.
[6] E. Guerrero, J. Brugues, J. Verdu, and P. de Paco, "Microwave microphone using a general purpose 24-GHz FMCW radar," *IEEE Sensors Letters*, vol. 4, no. 6, pp. 1–4, jun 2020.
[7] V. Chen, F. Li, S.-S. Ho, and H. Wechsler, "Micro-doppler effect in radar: phenomenon, model, and simulation study," *IEEE Transactions on Aerospace and Electronic Systems*, vol. 42, no. 1, pp. 2–21, jan 2006.
[8] S. Ram and H. Ling, "Microdoppler signature simulation of computer animated human and animal motions," in *2008 IEEE Antennas and Propagation Society International Symposium*. IEEE, jul 2008.
[9] R. Mamgain, R. Jain, and D. Deb, "Study and simulation of radar targets micro-doppler signature," in *2018 International Conference on Radar (RADAR)*. IEEE, aug 2018.
[10] J. Gong, J. Yan, D. Li, R. Chen, F. Tian, and Z. Yan, "Theoretical and experimental analysis of radar micro-doppler signature modulated by rotating blades of drones," *IEEE Antennas and Wireless Propagation Letters*, vol. 19, no. 10, pp. 1659–1663, oct 2020.
[11] Z. Zhou and J. Huang, "X-band radar cross-section of tandem helicopter based on dynamic analysis approach," *Sensors*, vol. 21, no. 1, p. 271, jan 2021.
[12] T. Peto, S. Bilicz, L. Szucs, S. Gyimothy, and J. Pavo, "The radar cross section of small propellers on unmanned aerial vehicles," in *2016 10th European Conference on Antennas and Propagation (EuCAP)*. IEEE, apr 2016.
[13] A. Lazaro, M. Lazaro, R. Villarino, and P. D. Paco, "New radar micro-doppler tag for road safety based on the signature of rotating backscatters," *IEEE Sensors Journal*, vol. 21, no. 6, pp. 8604–8612, mar 2021.
[14] A. Lazaro, M. Lazaro, R. Villarino, D. Girbau, and P. de Paco, "Car2car communication using a modulated backscatter and automotive FMCW radar," *Sensors*, vol. 21, no. 11, p. 3656, may 2021.
[15] W. Y. Yang, J. H. Park, J. W. Bae, N. H. Myung, and C. H. Kim, "Automatic algorithm for estimating the jet engine blade number from the radar target signature of aircraft targets," *IEEE Aerospace and Electronic Systems Magazine*, vol. 30, no. 7, pp. 18–29, jul 2015.
[16] *www.altair.com/feko*.
[17] V. Chen, "Analysis of radar micro-doppler with time-frequency transform," in *Proceedings of the Tenth IEEE Workshop on Statistical Signal and Array Processing (Cat. No.00TH8496)*. IEEE, 2020.

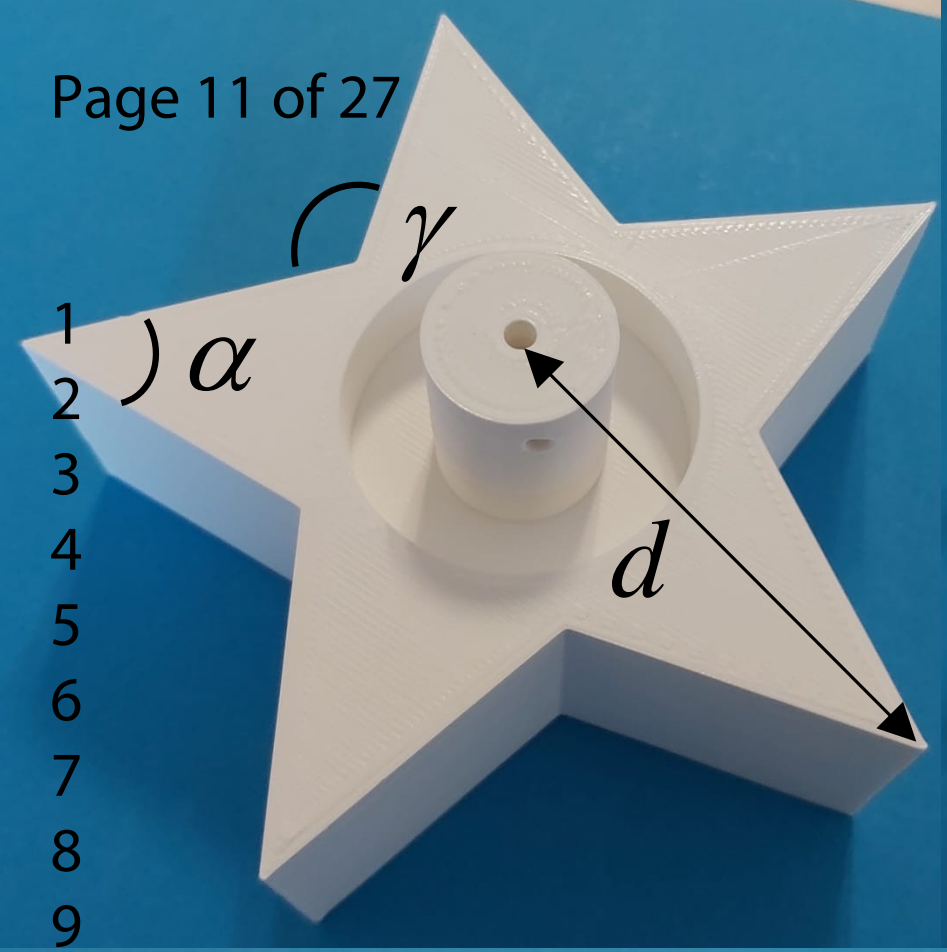
γ
α
d

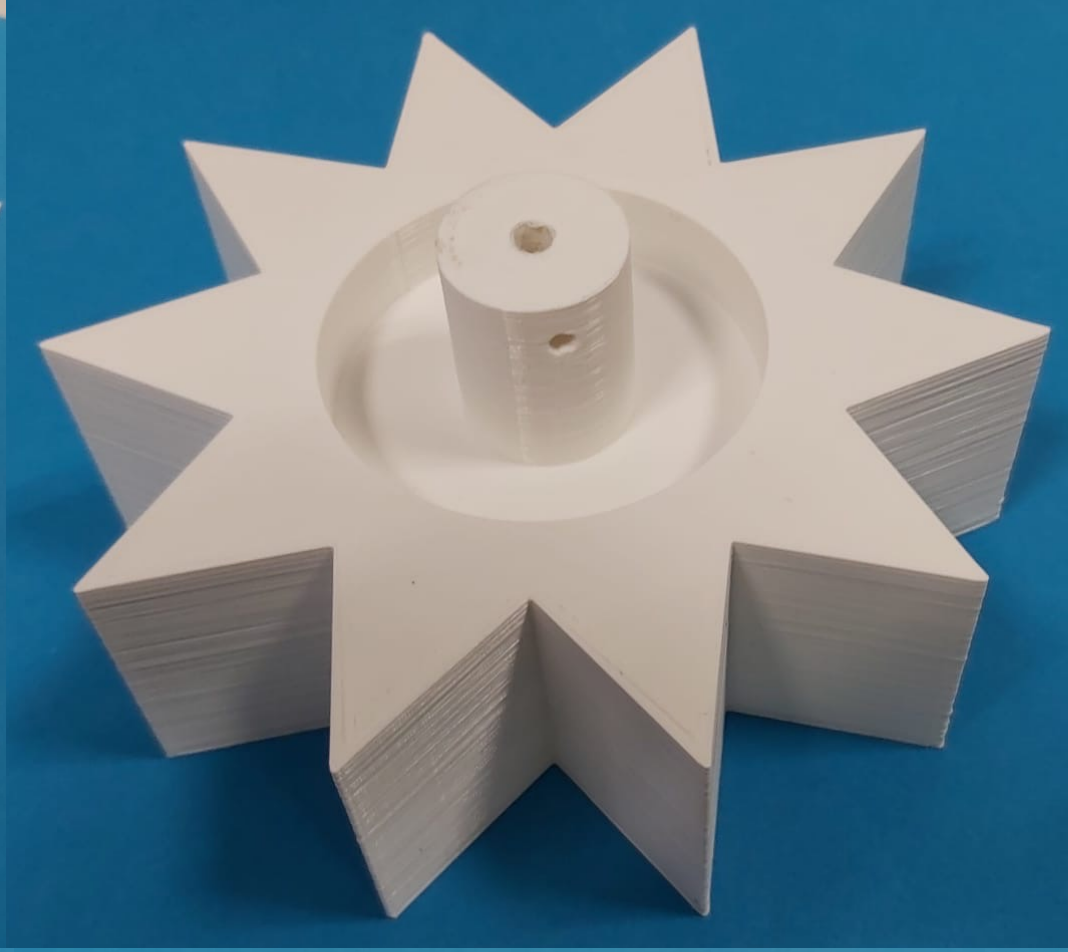

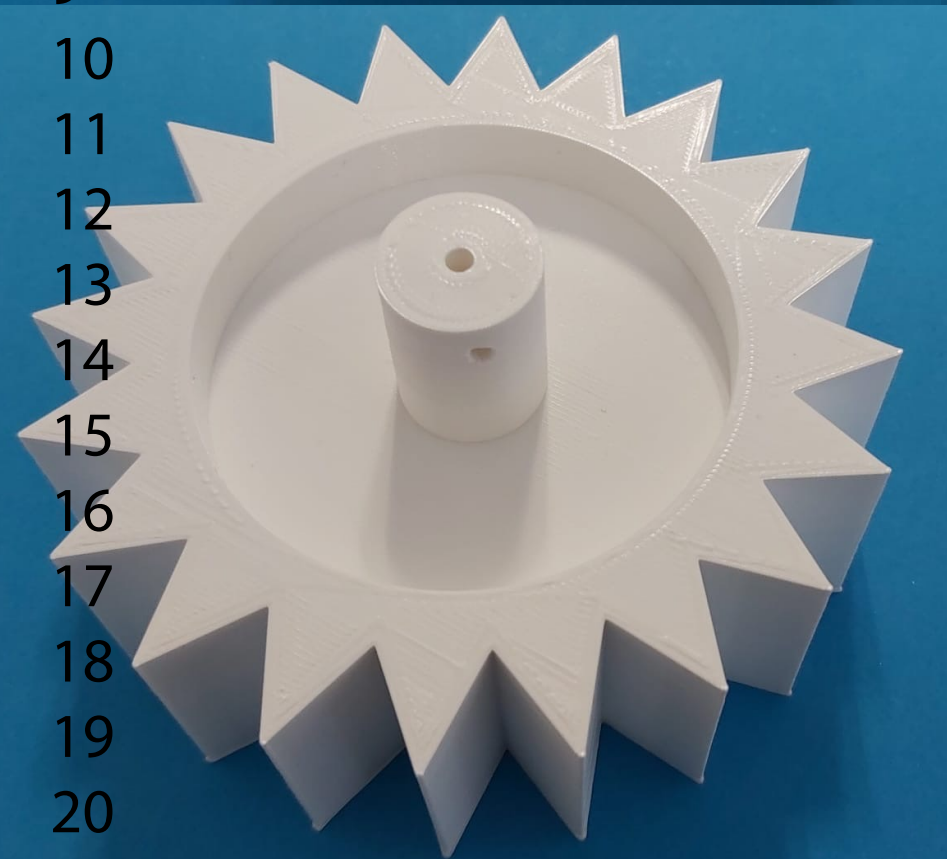

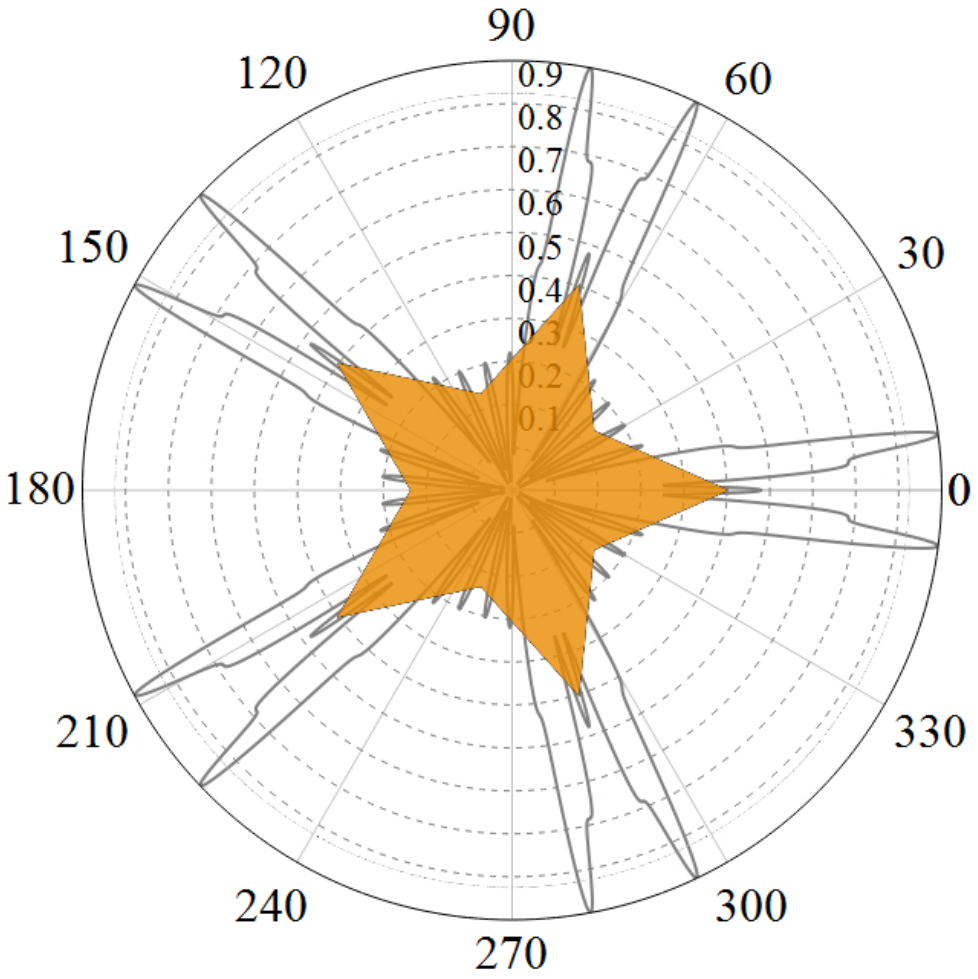

Normalised polar representation of the monostatic RCS for the (a) 5 tip

173x170mm (96 x 96 DPI)

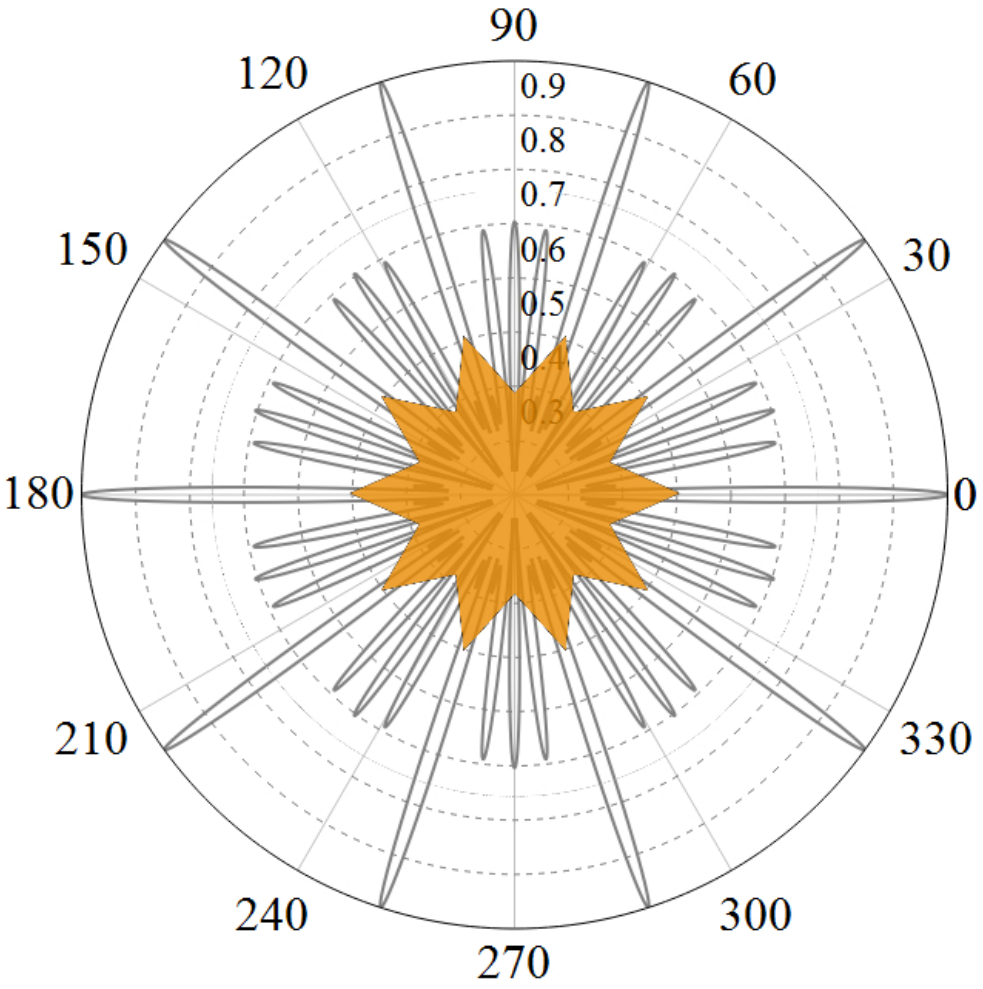

Normalised polar representation of the monostatic RCS for the (a) 10 tip

171x171mm (96 x 96 DPI)

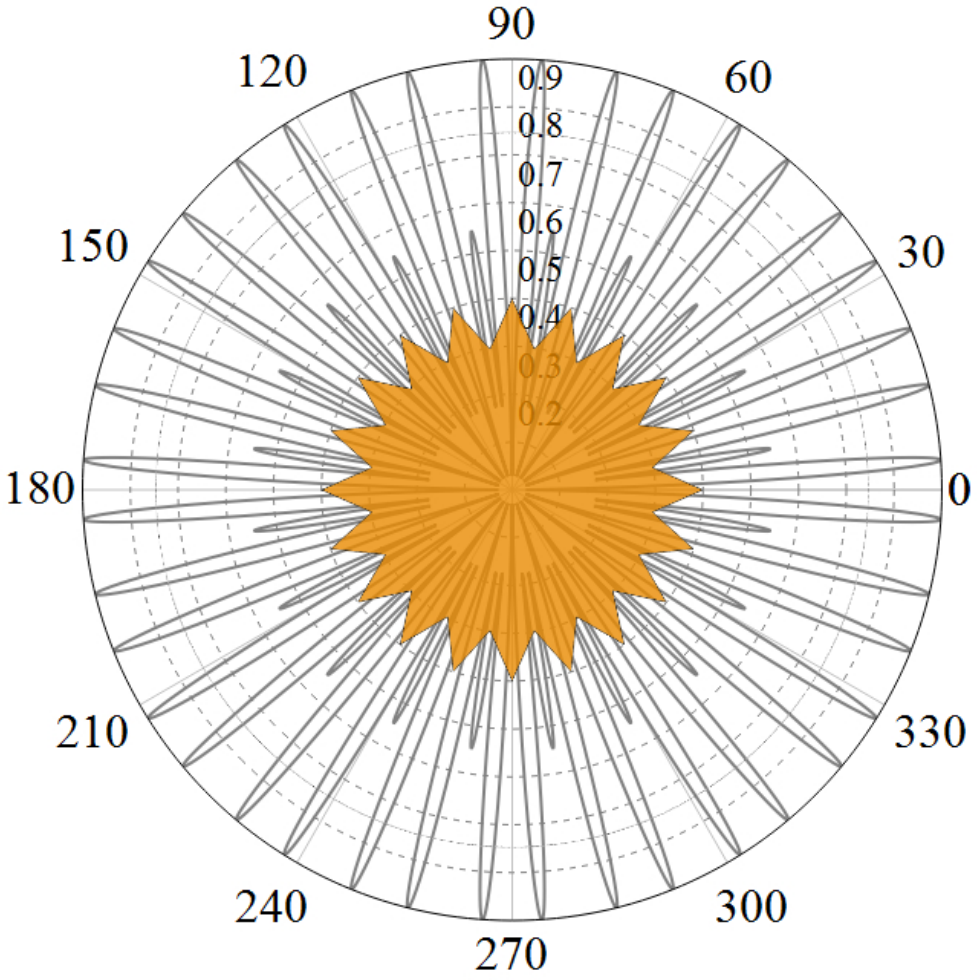

Normalised polar representation of the monostatic RCS for the (a) 20 tip

173x172mm (96 x 96 DPI)

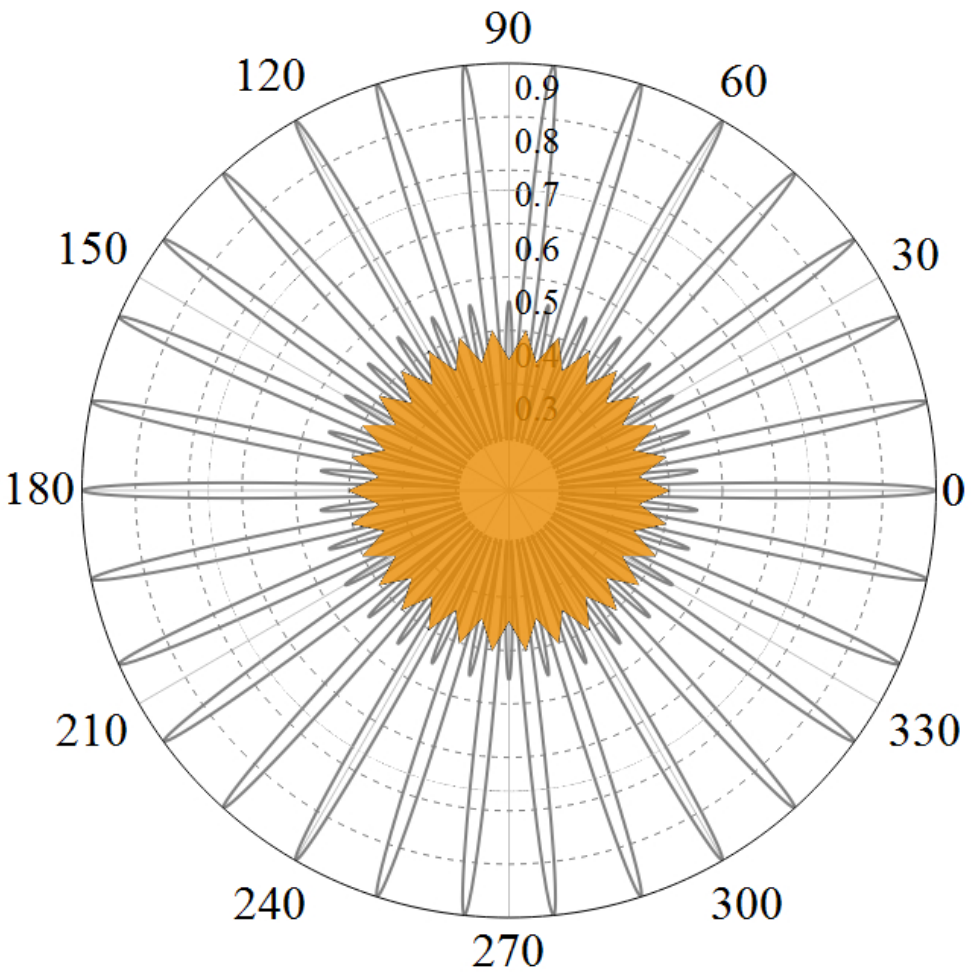

Normalised polar representation of the monostatic RCS for the (a) 30 tip

174x171mm (96 x 96 DPI)

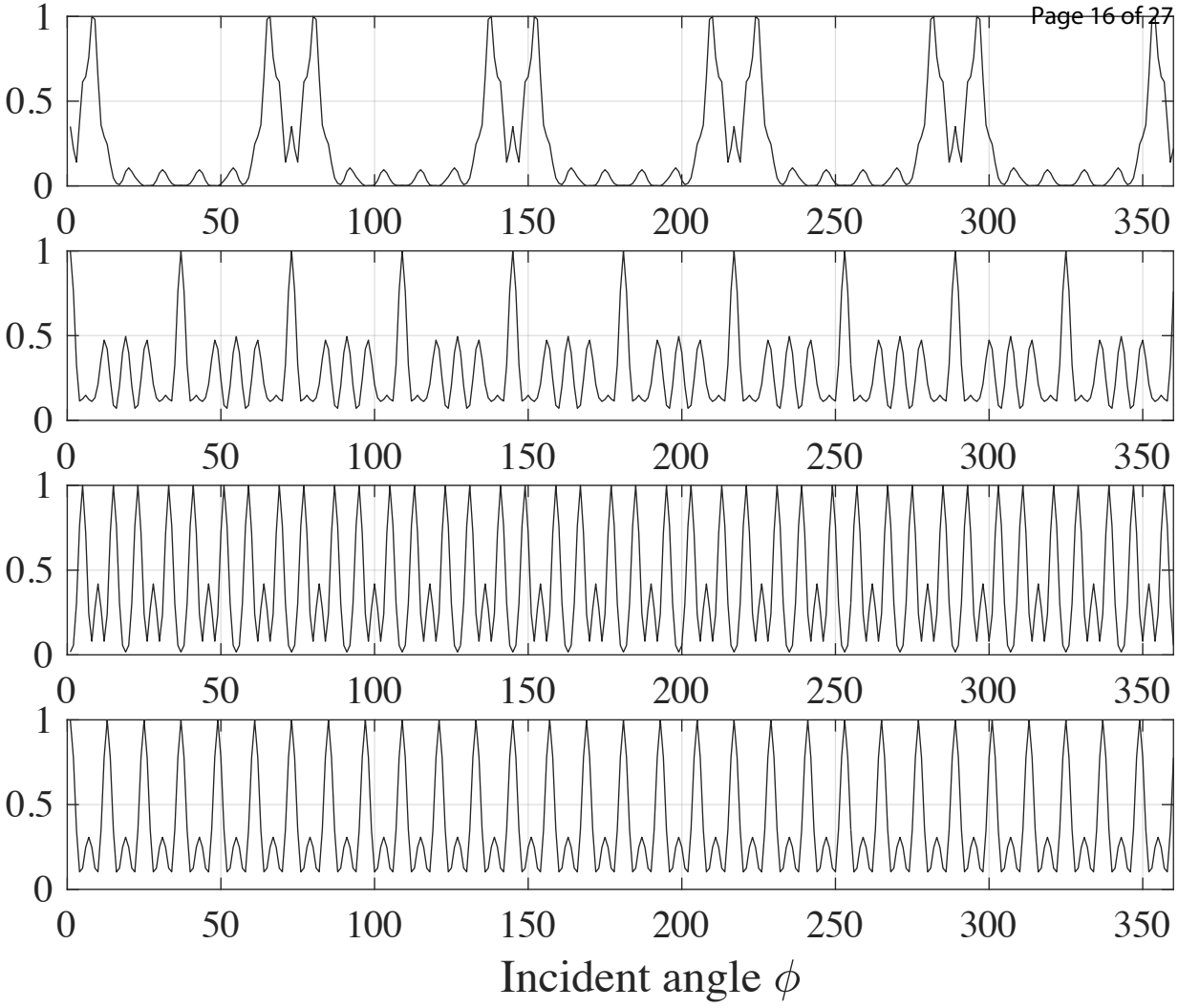
Modulation Waveform
1
0.5
0
0
50
100
150
200
250
300
350
Incident angle ϕ

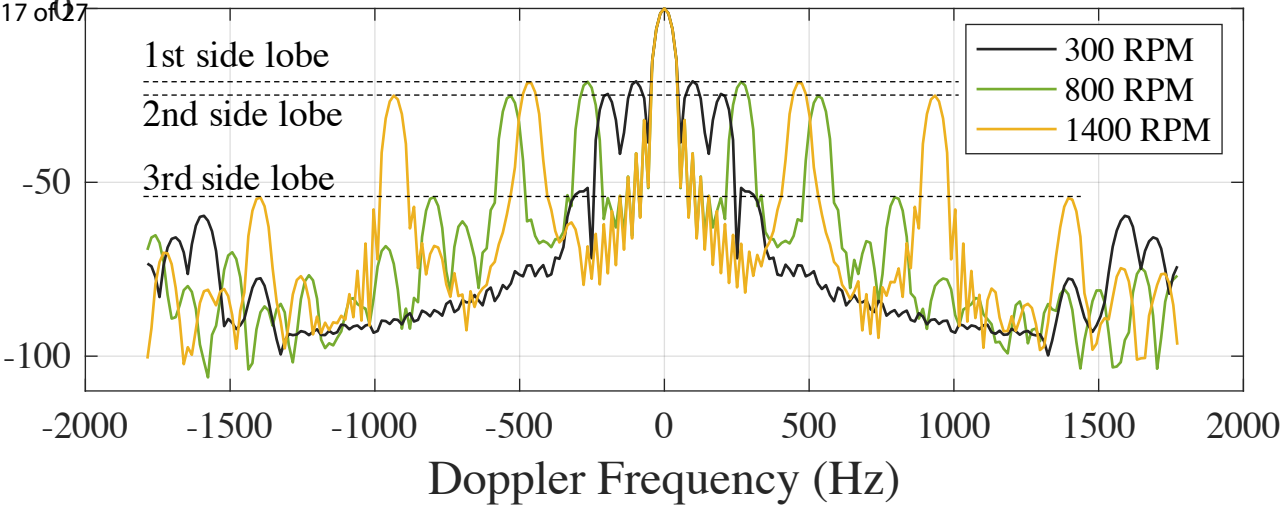
1st side lobe
2nd side lobe
3rd side lobe
300 RPM
800 RPM
1400 RPM
0
-50
-100
Normalized Level (dB)
-2000
-1500
-1000
-500
0
500
1000
1500
2000
Doppler Frequency (Hz)

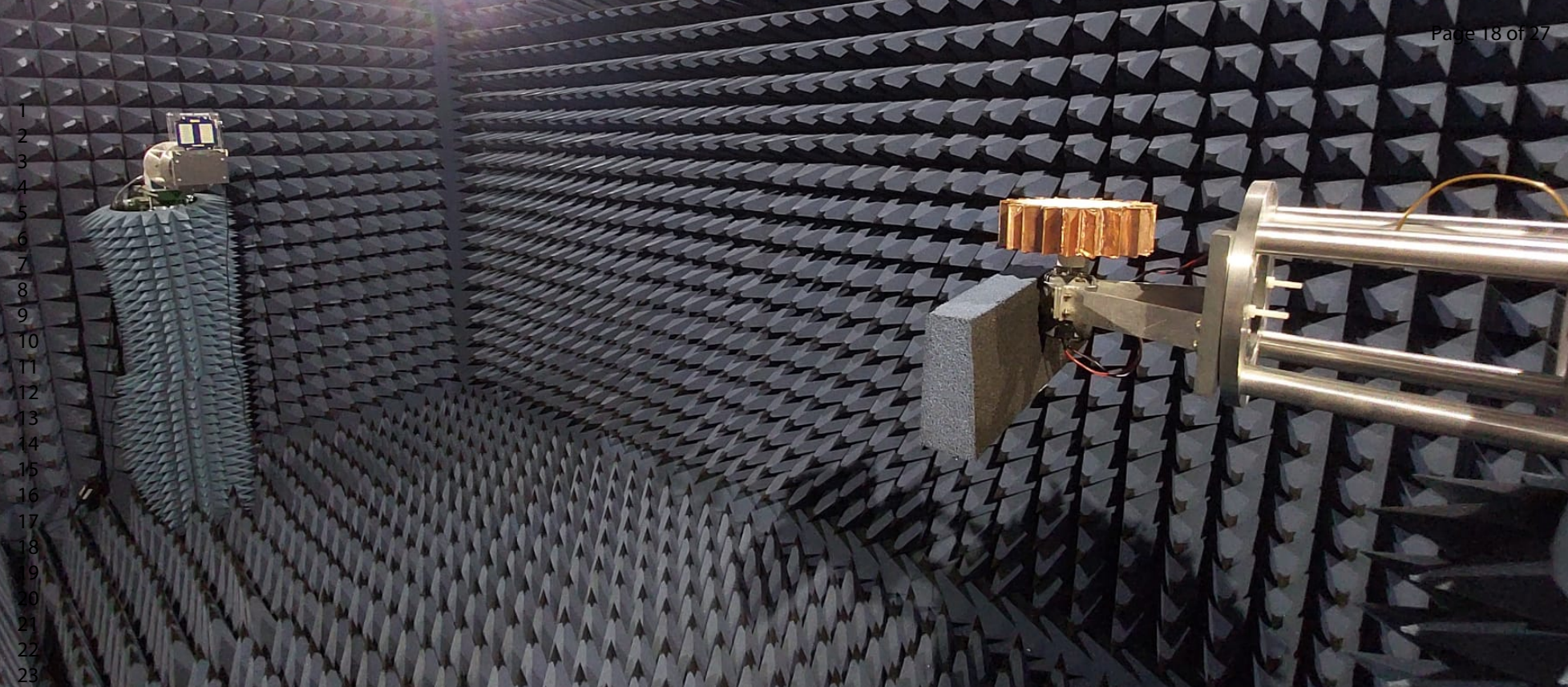

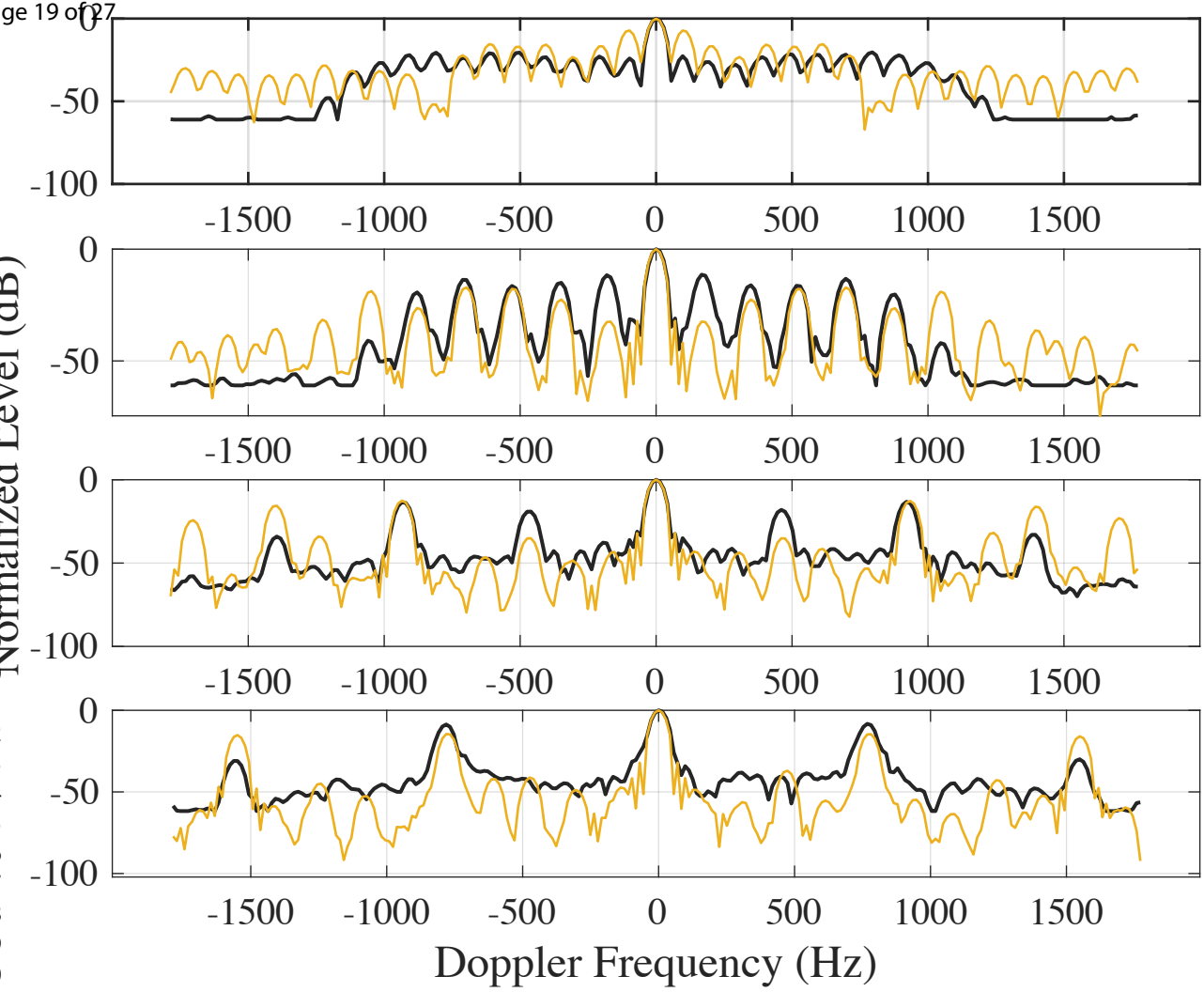
0
-50
-100
-1500
-1000
-500
0
500
1000
1500
Normalized Level (dB)
Doppler Frequency (Hz)

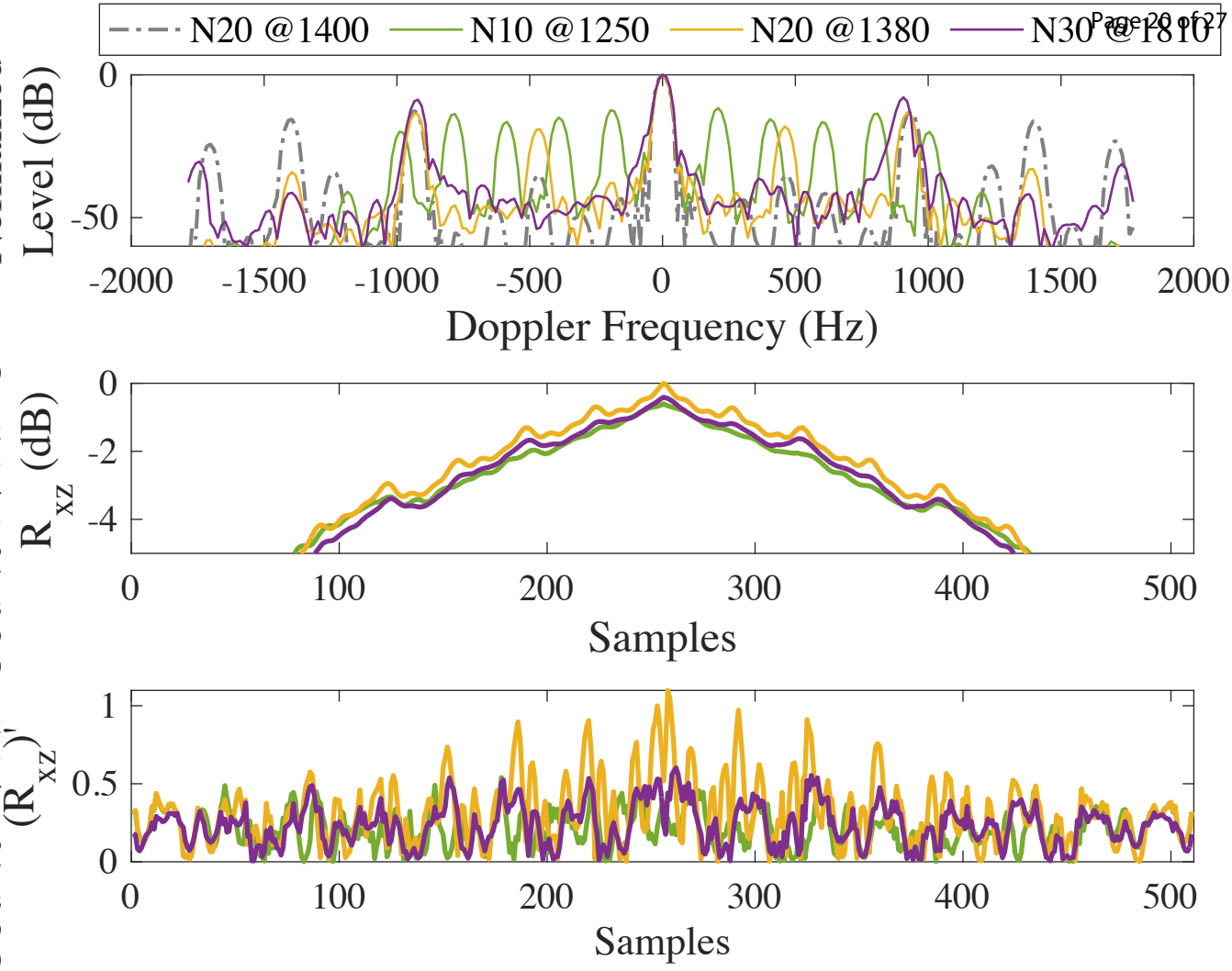
N20 @1400
N10 @1250
N20 @1380
N30 @1810
Normalized Level (dB)
0
-50
-2000
-1500
-1000
-500
0
500
1000
1500
2000
Doppler Frequency (Hz)
R_xz (dB)
0
-2
-4
0
100
200
300
400
500
Samples
(R_xz)'
1
0.5
0
0
100
200
300
400
500
Samples

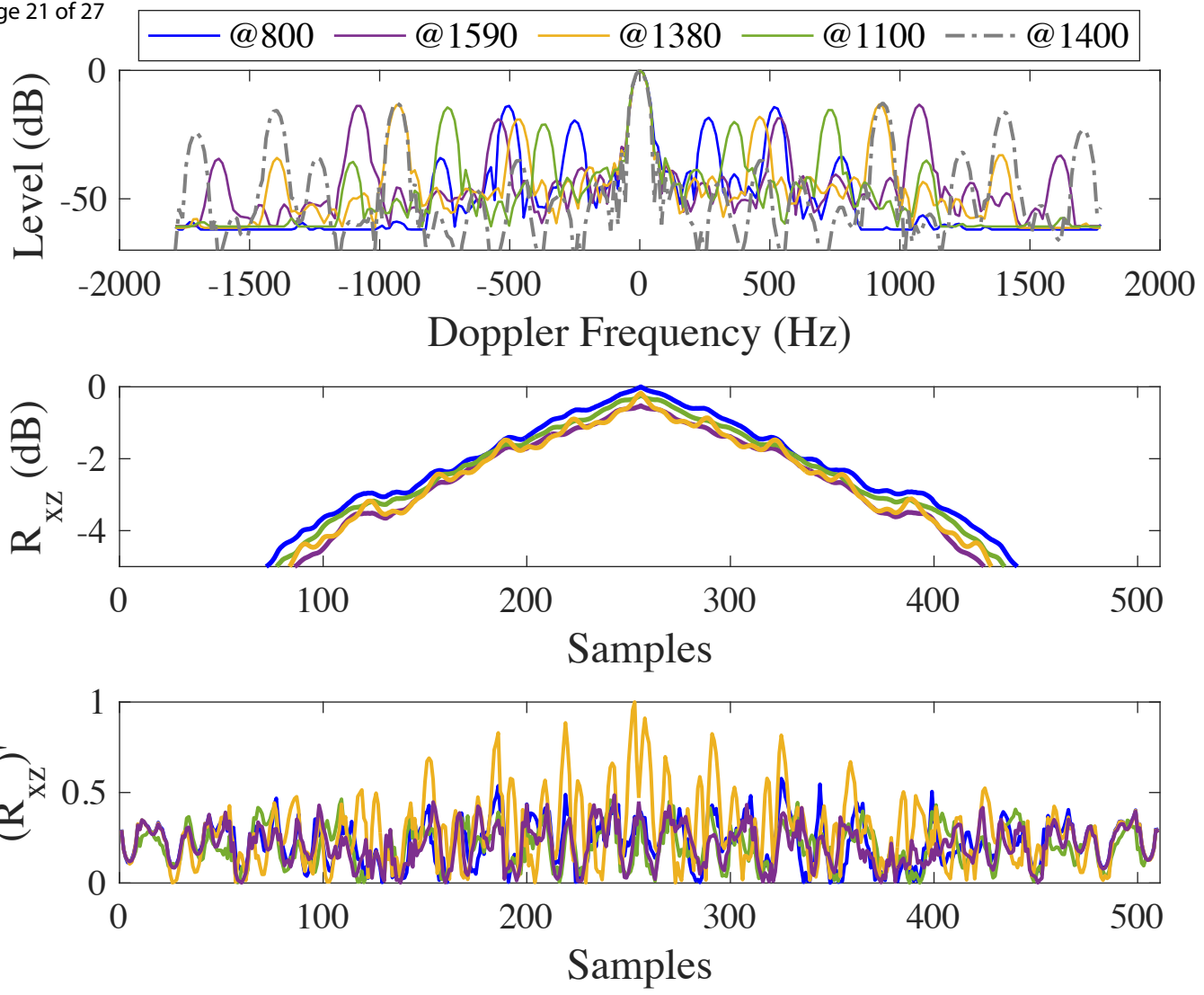
@800
@1590
@1380
@1100
@1400
Normalized Level (dB)
0
-50
-2000
-1500
-1000
-500
0
500
1000
1500
2000
Doppler Frequency (Hz)
R_{xz} (dB)
0
-2
-4
0
100
200
300
400
500
Samples
$(R_{xz})'$
1
0.5
0
0
100
200
300
400
500
Samples

Dear Associate Editor and Reviewers,
First, thanks a lot for the comments and suggestions. We strongly believe that the quality of the paper has been highly improved.

You can find the answer to your comments in blue color.

Best regards,

Associate Editor

Comments to the Author:
Please try to provide specific application and offer a slightly more complex structure in your analysis.

As it has been clarified in the introduction, the main application in which this work can be used is related to the generation of warning signals, specifically the rotating lighting signals. Considering that the modulating signal is given by the geometry of the rotating wheel, the detectability can be improved and the risk to suffer from spoofing attacks can be reduced. Compared with other solutions based on electronic modulation, the mechanical wheel is frequency-independent which can be determinant in applications in the band of 77 GHz. Following with the reviewer's comments, the well-known theoretical development has been substantially reduced and the discussion about detectability has been included as a new section.

Reviewer(s)' Comments to Author:

Reviewer: 1

Comments to the Author

This paper describes the use of rotating star shaped metallic objects as radar targets. While the use of artificial rotating radar targets might be new, the analysis and classification of the Doppler produced by rotating objects has been investigated before, (e.g. W. Y. Yang, J. H. Park, J. W. Bae, N. H. Myung and C. H. Kim, "Automatic algorithm for estimating the jet engine blade number from the radar target signature of aircraft targets," in IEEE Aerospace and Electronic Systems Magazine, vol. 30, no. 7, pp. 18-29, July 2015, doi: 10.1109/MAES.2015.140159. – no affiliation by the reviewer).

Thank you very much for your comments. It is true that the recognition of rotating objects by means of its microdoppler signature is not new and the theoretical developments can be found in the proposed paper by the reviewer. In this work, the novelty is given by considering that the modulating signal is due to the geometric shape of the rotating target. It has been validated the detectability for star-shaped rotating wheels.

The paper starts with an extremely simplified theoretical analysis in Section II that is not used throughout the paper.

Part of the section II has been removed since as the reviewer comment, it is a well-known theory which can be found in several references. We have focused the theoretical development in the consideration of a time-dependent RCS due to the geometric characteristics of the star-shaped wheel.

Instead the geometries are simulated in Feko and these simulations are used to build a model for the expected return signal (the authors call this “integrated RCS”?) given a short distance between radar and target.

We have reviewed the conditions for near and far-field considering the dimensions of the target as well as the operating frequency of the radar. With this, it has been found that the experiment is under far-field conditions. Therefore, as the reviewer suggested, the RCS to be used for the model is the monostatic which is not modified by the radiation pattern of the antenna.

The findings are rather trivial and no concrete connection to an application is presented.

As it has been included in the introduction, this work can be used for generating warning signals similarly to rotating lighting signals. In this case, as previously commented, it is advantageous that the application is frequency-independent since the modulating signal is given by the geometric shape.

The written English is difficult to follow and needs improvements.
Thanks for the comments. The English grammar has been carefully reviewed.

Specific comments

Section II is unclear. While Figure 2 depicts a star, the discussion seems to only assume scattering from the star tips? How is this justified?

The objective of modelling the star-shaped only considering backscatters in the tips was to provide a fast and easy model to analyze the received IF signal. However, this model is still far away from reality since it does not consider a time-dependent RCS. Following with the recommendation of the reviewer, the theoretical development in Section II has been highly simplified and merged with the analysis of the mechanical modulation in Section III. The Figure 2 has been deleted from the paper to avoid confusion in the used model. To do this, we have directly used the simulated time-dependent RCS.

Star is conductive? Please mention this earlier, e.g. in the abstract! This is particularly confusing since Fig. 1 shows the uncoated plastic wheels.

It is true that the wheels are not shown with the cooper adhesive layer in Figure 1. The justification is just for sake of clarity in the figure. However, in the introduction section it has been pointed that the wheels have been covered by the adhesive cooper layer.

“The wheels have been covered by an adhesive cooper layer to increase the reflectivity of the targets”.

“integrated RCS”: I do not understand the discussion in Section III. Why would the beamwidth of the RADAR antenna matter in the (true) far field? Does this analysis and Fig.4 assume a finite distance between the radar and the target? How large is it? Are you simply not in the far field? (The setup in Fig. 6 suggests that)

As it was suggested by the reviewer, the conditions to assume near or far field were studied and the conclusion is that, considering the target size as well as the distance between the radar and the target and the frequency operation of the radar it is more appropriate to use the far-field conditions. With this consideration, the RCS to be used must correspond to the monostatic, which

must not be modified by the beamwidth of the radar antenna. With this, as shown in Fig. 3, the new RCS to be considered have been modified as shown in the next figure

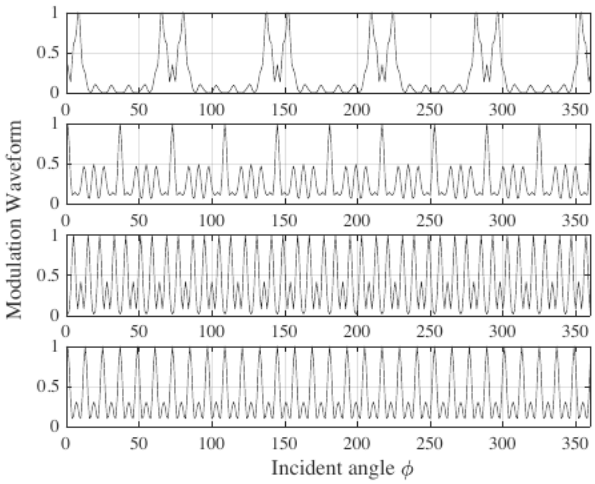

The comparison between simulation and measurement in Figure 6 (in the new paper version) has been also modified since the received signal is not the same as previous version since the used RCS is also different.

Discussion of the number of tips of the star shaped wheel vs. modulation spectra and rotation speed is rather trivial, especially since there is no further information on target bandwidths or other application related information given.

The discussion has been complemented with the section focused on the detection method. The comparison in Figure 4 is important since it shows that the amplitude of the first, second, third (and so on) lobes is not dependent on the rotation rate. This strength the proposed method to detect the expected signal as it has been included in Section IV. Some discussion is also provided in relation to the modulation bandwidth which depends on the rotation rate at the end of page 2:

"For Ωr = 300 RPM, the amplitude of the third side lobe is not perfectly aligned with the others as it occurs for higher rotation rates. This is due to the fact that this side lobe is approximately allocated in the limit of the modulation bandwidth which can be approximated as Bw ≈ 2(β + 1)Ωr /2π [13]. For Ωr = 300 RPM (5 Hz), the third (k = 3) side lobe is allocated at kΩr N = 300 Hz, being Bw ≈ 580 Hz (with d = 5.7 cm and f0 = 24 GHz)"

Detailed comments

Page 2, left column: "For sake of simplicity, a single rotating backscatter k = 1 depicted in Fig. 2 is first considered." This sentence is not clear. What is a single backsctatter? Do you mean a single scattering object? How does this relate to k?

As it was previously commented, and taking into consideration the advice of the reviewer, the Fig. 2 in the previous version of the paper has been deleted to avoid further confusions. The objective was to demonstrate that the model using single backscatters is not precise enough to properly model the reception of the IF signal.

Page 2, left column: "The previous development considers the star-shaped wheel modelled with single isolated backscatters in the tip's positions." This information is too late, should be discussed in section II.

The model using single backscatters has been highly simplified as the reviewer suggested. The section II has been focused on the use of mechanical modulation by means of time-dependent RCS which is more suitable to properly model the reception of the IF signal.

Page 3, right column “The 5, 10, 20 and 30 tip star-shaped wheels have been fabricated using low cost additive 3D manufacturing including, afterwards, a conductive adhesive layer.” Very hard to understand for native English speakers, guess this means that the pieces were 3D printed in a dielectric and afterwards coated with a conductive layer? What material was used for the coating?

We agree that the redaction was a little confusing. Therefore, in the introduction section a new phrase has been included stating that:

“The wheels have been covered by an adhesive cooper layer to increase the reflectivity of the targets”.

The used material for the coating was adhesive cooper.

Page 6, conclusion: “Characterization of different star-shaped wheels using a general purpose 24 GHz radar platform demonstrates and supports theoretical developments and simulation results.” What theory are you referring to? I do not see the theory of secion II used anywhere in the paper, or compared to it!

We agree with the reviewer and a new section IV has been included which discusses the method for detecting rotating star-shaped wheels. Since the application is focused on the generation of warning signals, we may know a priori what kind of IF signal we should expect. Thanks to the agreement between simulation and measurement, specifically in the allocation of lobes, in this work we have proposed the use of the derivative of the discrete cross-correlation between a reference signal (simulation) and the received signal (measured).
Since the allocation of lobes between measurement and simulation are coincident, the obtained cross-correlation reveals the presence of peaks where the difference between them corresponds to the product $N\Omega$. That is why, when the derivative is carried out, the presence of peaks is much stronger for the expected signal compared with other as shown in Fig. 7 in the new version of the paper. We believe that this result experimentally supports the findings.

Reviewer: 2

Comments to the Author

This is an interesting paper investigating the detection of different geometries for rotating targets by means of micro-Doppler signature. Specific geometric shapes are demonstrated to lead to a particular modulation waveform. It is suggested that the authors can answer the following questions.

Thanks a lot for the comments of the reviewer. All of them have been considered to improve the quality of the paper.

1. The measurement has shown good agreement for the allocation of frequency lobes with theoretical simulations in Fig. 7. However, big discrepancies are observed between 500 to 1000 Doppler frequencies for 10 tip star-shaped wheels @ 1100 RPM. The authors' explanation is not sufficient for these since other cases matches very well. It will be interesting if authors can investigate the reason.

As it has been previously commented for reviewer 1, it is true that the experiment should consider far-field conditions. Therefore, the monostatic RCS should be used instead the bistatic. This modifies the shape of the simulated IF signal.

After this, the comparison between the simulation and the measurement has been carried out in Fig. 6 in the new paper version. As in the previous version of the paper, there is some little discrepancies in the amplitude of the lobes. Finally, we have concluded that the amplitude of the lobes is very sensitive to external effects which are not considered in the simulation model. The main of those effects is related to vibrations of the rotating wheel in the elevation plane. Since the prototypes are made of PLA, the hole of the star-shaped wheel does not allocate the motor's axe and some vibration may appear due to this situation. This has been specified in the paper in the last paragraph of section III in the new version of the paper:

The discrepancy in the amplitude of some lobes may come from vibrations in the elevation plane due to some vibration in the plane of rotation non considered in the theoretical model.

2. The authors compare different tip star-shaped wheels at different RPM. Since the goal is to identify a certain rotating target, can the authors show the classification at the same RPM for different wheels?

Following with the recommendation of the reviewer, we have included a new section focused on the classification (detectability). As explained in the paper, when the number of tips is different and the rotation rate is the same, the allocation of the lobes will be also different compared with the reference level. To consider a more complicated scenario, we have selected rotation rate for the different wheels which yield in lobes which are coincident, some of them, with the reference signal. The cross-correlation of the reference signal with the different measurements is enough to detect the expected signal (the one with the same number of tips).

Moreover, we have carried out the same experiment for a wheel with the same number of tips but rotating at different rotation rates. This scenario yields a worst situation than previous one since the use of the cross-correlation is not enough to carry out the detection. That is why, the use of the derivative of the cross-correlation has been implemented which clearly overcomes this situation and thus, the detection can be completed.

Here the results are shown for both experiments (also shown in the new version of the paper Fig. 7). In both set of graphs, the reference signal should be correlated to the measured signal with 20 tips (case a), and 1380 RPM (case b). In both cases, this is the yellow trace.

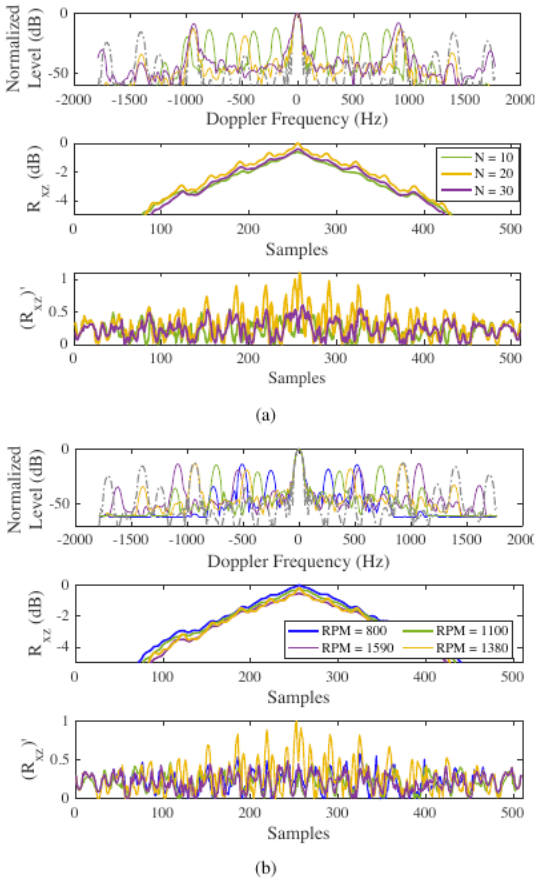

Fig. 7. (Top) Comparison between the reference signal (grey dot-dash line) and measured received signals, (middle) Cross-correlation between the reference signal and measurements, (bottom) derivative of the cross-correlation. (a) Results for star-shaped wheels with different number of tips N, (b) Results for a 20 tips wheel at different rotation rates.

3. This paper aims to characterize different star-shaped wheels using 24GHz radar platform. It is expected that the authors can explain how to distinguish different tips from Doppler signals in Fig. 7. The simulation results have many small ripples, which do not exist in measurement results. In such case, it is suggested if the authors can give algorithms to differentiate them. That will also show the reliability and robustness of this method.

As it has been answered in the previous comment, a new section has been included in the paper focused on the algorithm for detection of rotating star-shaped wheels. We believe that this shows the reliability and robustness of the method as suggested by the reviewer.
In relation with the small ripples, it has been seen that they are not as stronger as in the previous version of the paper. This is because, as commented in comment 1, now we have used the monostatic RCS which modifies the simulated received IF signal. In this sense, the shown ripples are not as strong as before. On the other hand, since no noise level has been considered in the simulation, there are different lobes which appears in the simulation below the noise level given in the measurement.